

Vladimir Molchanov

**The  $K^+ \rightarrow \pi^+ \nu \bar{\nu}$  measurement:  
simulations for the P940 geometry**

**Abstract**

Monte-Carlo simulations of the  $K^+ \rightarrow \pi^+ \nu \bar{\nu}$  acceptance, various backgrounds and rates in some detectors are presented. The note is written as a prototype of a "Simulations" chapter for a full scale proposal.

March 2005    Fermilab

# Contents

<b>1</b>	<b>Simulations</b>	<b>1</b>
1.1	Monte Carlo overview . . . . .	1
1.2	The $K^+ \rightarrow \pi^+ \nu \bar{\nu}$ decay . . . . .	4
1.3	Kaon decay backgrounds . . . . .	9
1.3.1	The $K^+ \rightarrow \mu^+ \nu$ background . . . . .	9
1.3.2	The $K^+ \rightarrow \pi^+ \pi^0$ background . . . . .	11
1.3.3	The $K^+ \rightarrow \pi^+ \pi^0 \gamma$ background . . . . .	16
1.3.4	The $K^+ \rightarrow \pi^+ \pi^- e^+ \nu$ background . . . . .	20
1.3.5	The $K^+ \rightarrow \pi^+ \pi^- \mu^+ \nu$ background . . . . .	28
1.3.6	The $K^+ \rightarrow \pi^+ \pi^+ \pi^-$ background . . . . .	28
1.3.7	Other kaon decay backgrounds . . . . .	30
1.3.8	Upstream $K^+$ decays backgrounds . . . . .	31
1.4	Accidental and interaction backgrounds . . . . .	36
1.4.1	Accidentals in the UMS . . . . .	36
1.4.2	Accidentals in the UMS and kaon RICH . . . . .	37
1.4.3	The $K^+$ residual gas interactions . . . . .	40
1.5	Rates in detectors and associated inefficiency . . . . .	41
1.5.1	Global inefficiency . . . . .	41
1.5.2	Rates in the DMS and FVS . . . . .	42
1.6	Summary . . . . .	46

# Chapter 1

## Simulations

We have performed Monte Carlo simulations to evaluate  $K^+ \rightarrow \pi^+ \nu \bar{\nu}$  acceptance, to study backgrounds and to estimate rates. We have benefited tremendously from the experience of P921 simulations. We have concentrated our efforts on issues which we know to be of importance, and which can be of importance because of differences in the P940 and P921 experimental techniques.

### 1.1 Monte Carlo overview

We have based the Monte Carlo program on GEANT-3.21. However, we use it like a ray trace, with all processes disabled, except those relevant for performed studies. Such an approach provides visual control over geometry, protects against trivial mistakes in tracking, and gives flexibility to selectively employ full GEANT power where necessary.

We have implemented only a part of the P940 apparatus, which is shown in Fig. 1.1. Origin of the coordinate system is put at the production target. No magnets and detectors of the upstream magnetic spectrometer (UMS) are simulated. Beam particles are generated at the  $Z$  position of the last UMS station. After that point we have made fairly good (within 10–20%) description of material traversed by charged particles in the acceptance of the apparatus.

Shape of the vacuum vessel is believed to fit into KTeV hall. Main elements of the simulated setup are beam veto system (BVS), vacuum veto system (VVS), forward veto system (FVS), surrounding veto system (SVS), muon veto system (MVS), magnet with  $p_T = 0.120$  GeV, straw tubes of the downstream magnetic spectrometer (DMS), kaon and pion RICHes. There are helium bags upstream of the kaon RICH and between vacuum vessel and pion RICH. A 10 cm in diameter beam pipe goes through the apparatus starting from the vacuum vessel. There are 13 modules of the VVS, the last 2 of which are, contrary to the name, located in air. We have assumed to employ KTeV CsI calorimeter as the FVS. However, it is not able to cover all the required aperture, that is why we use SVS just upstream of the FVS.

Beam particles are generated as going along the axis of the apparatus with  $\sigma(x) = \sigma(y) = 1$  cm and  $\sigma(\theta_x) = \sigma(\theta_y) = 0.2$  mrad. At that point reconstructed parameters of the primary

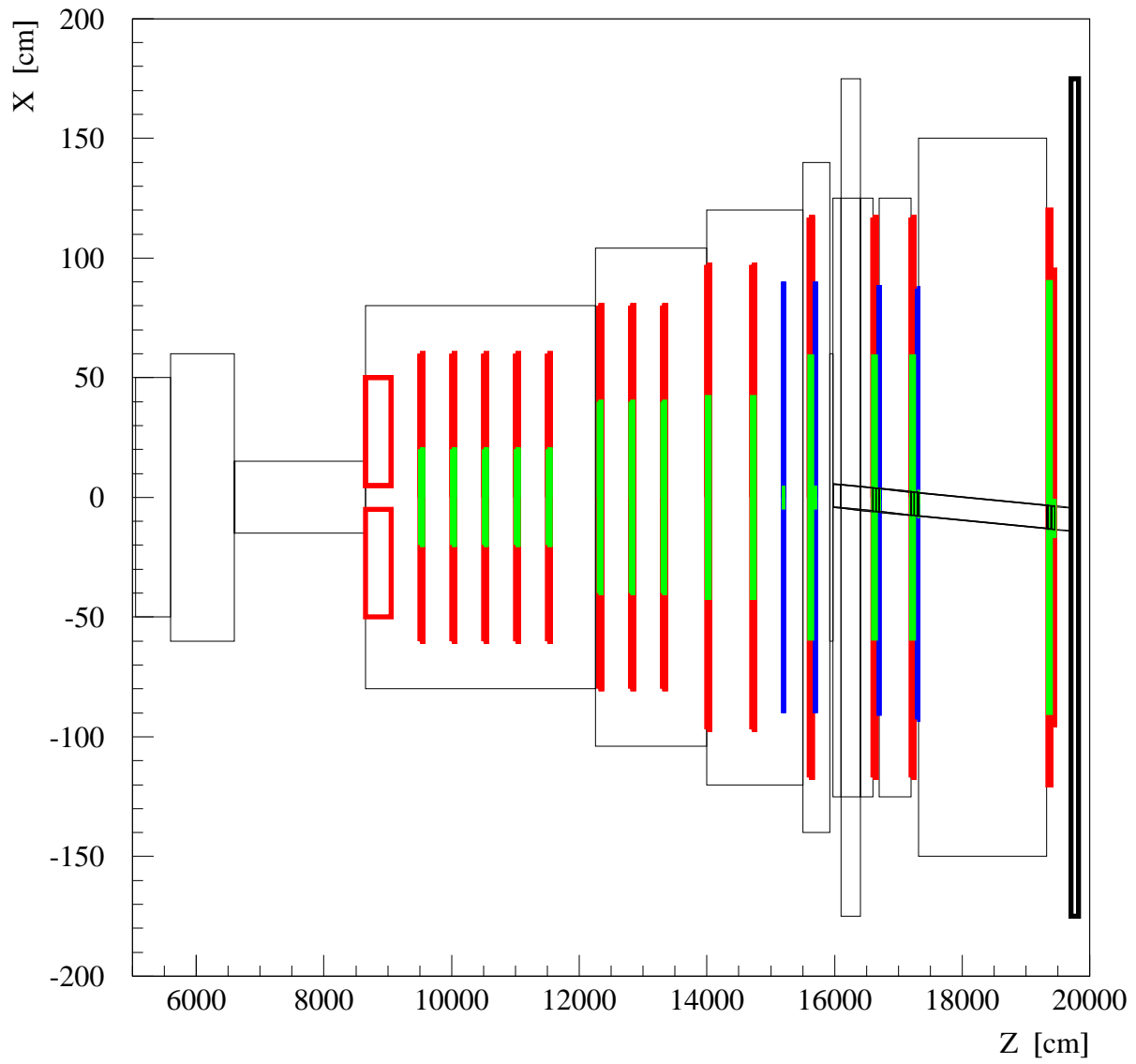


Figure 1.1: Downstream part of the P940 apparatus.

track are parameterized using normal resolution functions with following parameters [1]:

$$\sigma(p)/p = 0.36524 \cdot 10^{-3} + 0.51123 \cdot 10^{-4} \times p \quad (1.1)$$

$$\sigma(\theta_x) = 30.455 \cdot 10^{-6} - 0.230 \cdot 10^{-6} \times p \quad (1.2)$$

$$\sigma(\theta_y) = 32.125 \cdot 10^{-6} - 0.091 \cdot 10^{-6} \times p \quad (1.3)$$

where  $p$  is momentum and measured in GeV. Beam track measurement in the kaon RICH is parameterized using its velocity vector at the entrance of the detector and smearing with normal distribution. Kaon RICH resolutions have been studied in stand-alone simulations [2], and then crudely parameterized as follows:

$$\sigma(p)/p = 0.70 \cdot 10^{-2} + 0.35 \cdot 10^{-2} \times (p - 37)/(53 - 37) \quad (1.4)$$

$$\sigma(\theta_x) = \sigma(\theta_y) = 0.165 \cdot 10^{-3} - 0.065 \cdot 10^{-3} \times (p - 37)/(53 - 37) \quad (1.5)$$

where  $p$  is calculated from velocity assuming the particle is a kaon, and is measured in GeV. Kaon RICH angular resolution is slightly better than beam divergence and much worse than the magnetic spectrometer measurement. For the reconstruction of secondary charged tracks we assume that each DMS station has a  $2X2Y2U2V$  structure, with no tubes in the 10 cm central region to allow for beam. It is required that a track traverses at least 5 planes in each DMS station. No pattern recognition is attempted. Hits are digitized using  $\sigma = 150 \mu\text{m}$  gaussian resolution and fitted to a simple model of track kink in the center of magnet. We have found that typical DMS resolutions are  $\sigma(\theta) \approx 32 \cdot 10^{-6}$  and  $\sigma(p)/p \approx 0.01$ . Pion RICH response is parameterized using resolution functions, calculated from stand-alone RICH studies [2]:

$$\sigma(p)/p = 0.759 \cdot 10^{-2} - 0.619 \cdot 10^{-3} \times p + 0.394 \cdot 10^{-4} \times p^2 - 0.110 \cdot 10^{-6} \times p^3 \quad (1.6)$$

$$\sigma(\theta_x) = \sigma(\theta_y) = \frac{-0.661 \cdot 10^{-3} + 0.951 \cdot 10^{-4} \times p - 0.582 \cdot 10^{-5} \times p^2}{11.5 - p} \quad (1.7)$$

where  $p$  is measured in GeV. To simulate photon veto rejection we track photons until a veto module is hit. At that moment the particle is stopped. Later, using saved value of particle's energy, veto inefficiency is determined by lookup in accordance with Table 1.1. Thus for such kind of study actual structure of the photon veto modules is irrelevant. Similarly, no simulation of the MVS is performed. However, we assume it to be sufficiently large to cover all the available acceptance.

Energy [GeV]	VVS <sub>1-5</sub>	VVS <sub>6-13</sub>	SVS	FVS	Beam Hole	Near $\pi^+$
0.0 — 0.060	1	1	1	1	1	1
0.060 — 0.120	1	$7 \cdot 10^{-4}$	1	1	1	1
0.120 — 0.200	$4 \cdot 10^{-4}$	$4 \cdot 10^{-4}$	$4 \cdot 10^{-4}$	1	1	1
0.200 — 0.700	$1 \cdot 10^{-4}$	$1 \cdot 10^{-4}$	$1 \cdot 10^{-4}$	1	1	1
0.700 — 1.0	$1 \cdot 10^{-5}$	$1 \cdot 10^{-5}$	$1 \cdot 10^{-5}$	$1 \cdot 10^{-5}$	1	1
1.0 — $\infty$	$1 \cdot 10^{-5}$	$1 \cdot 10^{-5}$	$1 \cdot 10^{-5}$	$3 \cdot 10^{-6}$	1	1

Table 1.1: Photon veto inefficiencies, used in simulations, as a functions of photon energy and detector hitted. A photon is considered to be near  $\pi^+$  if the distance between them is less than 10 cm at the front of the FVS.

## 1.2 The $K^+ \rightarrow \pi^+ \nu \bar{\nu}$ decay

With present day technology one can not hope to select the  $K^+ \rightarrow \pi^+ \nu \bar{\nu}$  decay in the kinematic region where  $K^+ \rightarrow \pi^+ \pi^0$  would contribute when  $\pi^0$  is lost. That is why a notion of regions I and II has been introduced. Region I refers to events with missing mass squared below the  $m_{\pi^0}^2$ , region II refers to events with missing mass squared above that value.

### Matrix element

We generate  $K^+ \rightarrow \pi^+ \nu \bar{\nu}$  decays with  $K_{e3}$  matrix element and form factor. Compared to uniform over the phase space distribution, it leads to about 50% increase in acceptance for region I and 10% for region II.

### Event reconstruction and selection

Event selection procedure basically follows that of the previous studies of the P921 [3]. There are aperture cuts, event kinematics cuts, and reconstruction quality cuts. The cuts were selected to provide reasonable kinematic resolutions and high overall efficiency. No doubt, there is room for improvement both in geometry of the experimental setup and in details of the event selection. However, at present stage of investigations optimization is definitely premature. All steps in the event selection are listed below. Since we simulate only the most significant features in each process, many selection criteria are automatically satisfied, while in real life efficiency would be below 100%. This must be remembered when calculating the overall efficiency or the final number of registered events.

Primary track is required to be reconstructed in the UMS and kaon RICH. Momenta, measured in the magnetic and velocity spectrometers, are required to be within 2.5% of each other:  $|1 - P_{\text{mag}}/P_{\text{vel}}| < 0.025$ , while their average has to be between 37 and 53 GeV. In the framework of performed simulations all these conditions are always satisfied.

Secondary track is required to be reconstructed in the DMS and pion RICH. The track is considered reconstructible in the pion RICH as long as it enters the detector. The track is reconstructed in the DMS if it produces hits in at least 6 planes in each DMS station and has acceptable quality:  $\chi_{\text{DMS}}^2/\text{d.o.f.} < 2.5$ . Momenta, measured in the magnetic and velocity spectrometers, are required to be within 5% of each other:  $|1 - P_{\text{mag}}/P_{\text{vel}}| < 0.05$ , while their average has to be between 14 and 30 GeV.

We also require consistency between missing masses, measured by the downstream magnetic and velocity spectrometers:  $|\text{MM}_{\text{mag}}^2 - \text{MM}_{\text{val}}^2| < 0.01 \text{ GeV}^2$ , while for the primary track the upstream magnetic spectrometer measurement is used, which is significantly more precise than the kaon RICH measurement. Thus the DMS and the pion RICH are required to agree twice: on the momentum and on the missing mass. Since both spectrometers measure momentum vectors, there is effectively one more constraint in reserve.

To suppress processes with muons, we require secondary track to be identified as a pion in the MVS.

Given the primary track has been reconstructed in the UMS and secondary track has passed through sufficient number of planes in the first two DMS stations, the decay vertex

is reconstructed. It is required to be of reasonable quality  $\chi_{\text{VTX}}^2 < 8.0$  and in the vicinity of the beam axis:  $\sqrt{X^2 + Y^2} < 6$  cm.

Thus far event selection criteria have been the same for region I and II. However, this need not be so, since background processes contribute differently to the regions. We define region I as corresponding to  $-0.004 < \text{MM}^2 < 0.008 \text{ GeV}^2$ , and region II as  $0.032 < \text{MM}^2 < 0.048 \text{ GeV}^2$ . We believe two processes limit region II missing mass upper boundary:  $K^+ \rightarrow \pi^+\pi^+\pi^-$  and  $K^+ \rightarrow \pi^+\pi^-e^+\nu$ . The minimal missing mass squared in  $K^+ \rightarrow \pi^+\pi^+\pi^-$  decay is  $(2m_{\pi^+})^2 = 0.078 \text{ GeV}^2$ . Taking into account resolution effects, this sets region II upper limit near  $0.068 \text{ GeV}^2$ . However, background from  $K^+ \rightarrow \pi^+\pi^-e^+\nu$  is even more restrictive. Study of it has shown that this background steeply rises with missing mass, and to keep it to acceptable level we use  $0.048 \text{ GeV}^2$  as region II upper boundary.

Vertex  $Z$  coordinate is required to be in the  $9100 < Z < 15000$  cm range for region I, and in smaller range of  $9100 < Z < 13500$  cm for region II. Again, this is to keep  $K^+ \rightarrow \pi^+\pi^-e^+\nu$  background under control.

Finally, it is required that there are no extra hits in some detectors, except those produced by the primary  $K^+$  and secondary  $\pi^+$ . These detectors include photon vetoes (BVS, VVS, SVS and FVS) and DMS straw tubes. No inefficiency could have possibly arisen in the performed simulations. In experiment we can expect inefficiency, associated with self-vetoing in the FVS due to fluctuations of the pion showers, and inefficiency, associated with accidental hits, which we further refer to as a global inefficiency. Of course, the latter strongly depends on the thresholds. Again, study of  $K^+ \rightarrow \pi^+\pi^-e^+\nu$  suggests that lower thresholds are required for region II (in particular, it may be necessary to set 1 MIP threshold in some part of the FVS). This means higher global inefficiency for region II.

## Results

We define acceptance as ratio of the number of events which passed event selection cuts to number of decays in the fiducial decay volume, which we define as the region from 9100 to 15000 cm. We have obtained 3.5% for acceptance in the region I and 5.0% for acceptance in the region II. As it has been said earlier, region II is subject to higher global inefficiency, so both regions seem to be of roughly equal importance.

Kaon and pion momenta, vertex  $Z$  coordinate and reconstructed missing mass squared for selected region I events are shown in Fig. 1.2. Same distributions for the region II are shown in Fig. 1.3. Average resolution on vertex  $Z$  coordinate for accepted events has been found to equal 26 cm. Combined missing mass squared resolution is  $1.83 \cdot 10^{-3} \text{ GeV}^2$  for region I and  $1.55 \cdot 10^{-3} \text{ GeV}^2$  for region II. One can get an impression of individual spectrometer contributions and multiple scattering effects using Table 1.2, where missing mass squared resolutions for different reconstruction methods are collected.

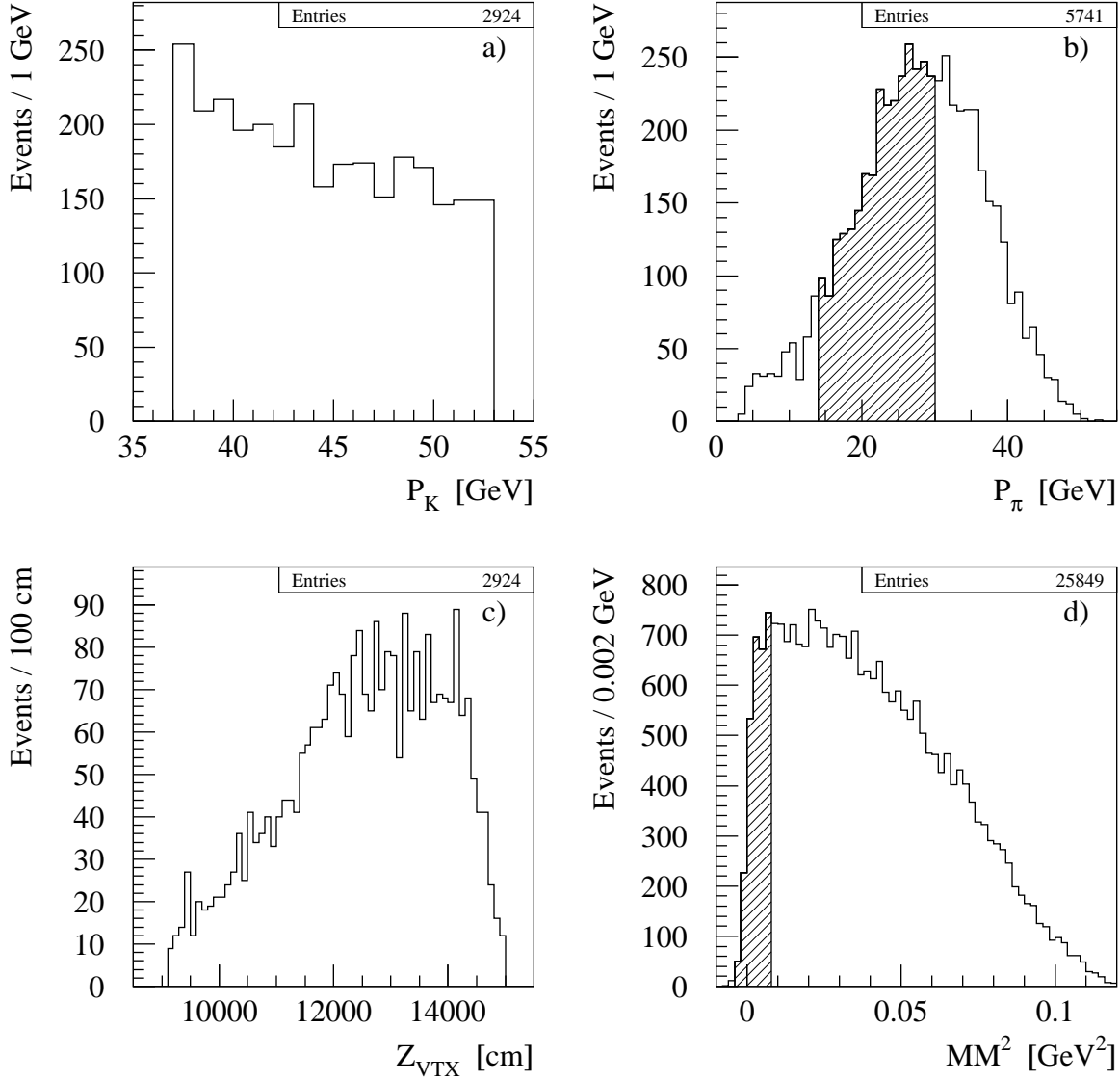


Figure 1.2:  $K^+ \rightarrow \pi^+ \nu \bar{\nu}$  region I distributions for selected events. In plots b) and d) final distribution is shown hatched, while histogram shows distribution with all cuts applied except that on the variable itself.

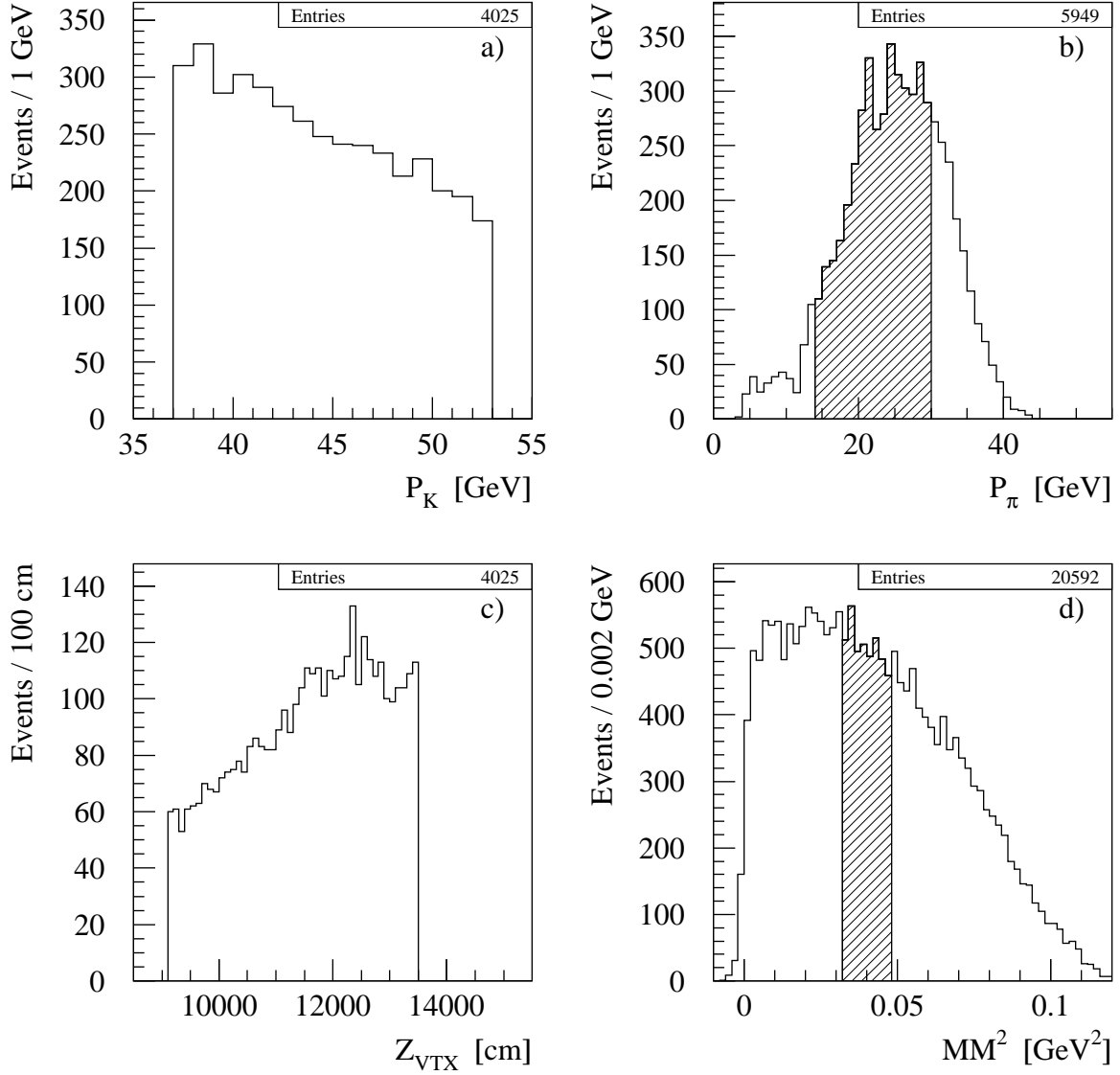


Figure 1.3:  $K^+ \rightarrow \pi^+ \nu \bar{\nu}$  region II distributions for selected events. In plots b) and d) final distribution is shown hatched, while histogram shows distribution with all cuts applied except that on the variable itself.

Reconstruction		With multiple scattering		Without multiple scattering	
$K^+$	$\pi^+$	Region-I	Region-II	Region-I	Region-II
Mag	—	0.53	0.43	0.47	0.40
Vel	—	2.55	1.97	2.52	2.03
—	Mag	1.84	1.53	1.02	0.80
—	Vel	3.71	3.11	3.55	2.87
Mag	Mag	1.92	1.59	1.13	0.91
Mag	Vel	3.67	3.10	3.59	2.94
Vel	Mag	3.13	2.53	2.76	2.18
Vel	Vel	4.47	3.65	4.27	3.53

Table 1.2: Missing mass squared resolutions in units of  $10^{-3} \text{ GeV}^2$ . Long dash indicates that true values have been used for mass calculation.

## 1.3 Kaon decay backgrounds

In this section we consider possible backgrounds caused by  $K^+$  decays. We have paid special attention to decays with large branching ratios and to decays which have been identified potentially problematic in our P921 studies [3].

As a matter of convention, we give background estimates in terms of an "effective branching ratio", defined as

$$\text{EBR} = \frac{\text{BR}[\text{process}] \times \text{Efficiency}[\text{process}]}{\text{Efficiency}[K^+ \rightarrow \pi^+ \nu \bar{\nu}]} \quad (1.8)$$

Thus signal/background ratio is simply  $\text{EBR}/\text{BR}[K^+ \rightarrow \pi^+ \nu \bar{\nu}]$ . A good feature of EBR is that it is more robust than an absolute background rate, because global inefficiency effects mostly cancel.

### 1.3.1 The $K^+ \rightarrow \mu^+ \nu$ background

The  $K^+ \rightarrow \mu^+ \nu$  decay is the most probable  $K^+$  decay with the branching ratio of 63.5%. Thus it is potentially a serious background to  $K^+ \rightarrow \pi^+ \nu \bar{\nu}$ . One of the design principles of the P940 experiment is an ability to suppress any major background by at least two independent ways. The  $K^+ \rightarrow \mu^+ \nu$  background can be rejected by vetoing muon in the MVS, by comparing momentum and velocity measurements of the muon, and by employing two-body kinematics. Muon rejection with the MVS is largely independent of two other possibilities. Usage of two-body kinematic constraint depends, however, on the reconstructed momentum (velocity). Thus it is fair to say that there are  $2^{1/2}$  independent ways to reject this background.

Let us consider muon momentum measurements in the magnetic and velocity spectrometers, momentum in the latter being reconstructed assuming the particle is a pion. Since the true particle identity is a muon, obvious relation holds:  $P_{\text{mag}}/P_{\text{vel}} = m_{\mu^+}/m_{\pi^+} \approx 0.76$ . Significant rejection of the background comes from the requirement of both measurements to agree within 5%:  $|1 - P_{\text{mag}}/P_{\text{vel}}| < 0.05$ . Since relative accuracy of both measurements lowers with momentum, high momentum muons are most likely to pass that selection. But even for maximal accepted momentum of 30 GeV the two momentum values are still  $7\sigma$  apart. Consequently, only non-gaussian effects can be a source of background. We have considered two extreme scenarios of incorrect measurements in either magnetic or velocity spectrometer only.

#### Incorrect magnetic spectrometer measurement

This scenario assumes basically correct measurement in the velocity spectrometer and significant mismeasurement in the magnetic spectrometer, so that its value for momentum falls within 5% of the velocity spectrometer measurement. This can happen due to multiple scattering in the DMS. In that case the measured missing mass squared equals to

$$\text{MM}^2 = -m_{\pi^+} (m_{\pi^+} - m_{\mu^+}) \left( \frac{m_{K^+}^2}{m_{\pi^+} m_{\mu^+}} - 1 \right) \approx -0.073 \text{ GeV} \quad (1.9)$$

Thus, for the event to look like a  $\pi^+\nu\bar{\nu}$ , it is also necessary either the primary kaon or the muon angle to be significantly mismeasured, while vertex selection criteria are still satisfied. We have simulated  $166\cdot 10^6$  events, allowing multiple scattering to evolve naturally. No event has passed region I selection criteria. Thus, the effective branching ratio limit is:

$$\text{EBR} < 1.1\cdot 10^{-7} \times \text{Efficiency}[\text{MVS}] \quad (1.10)$$

In fact, only one event has made all the way to get to a mass plot but failed the region I missing mass squared cut. True muon momentum in this event is 23.0 GeV, while reconstructed by momentum spectrometer is 27.7 GeV, and reconstructed by velocity spectrometer (assuming the track is pion) is 28.1 GeV. Combined missing mass squared equals  $-0.052 \text{ GeV}^2$ .

Very low background level can be understood by following argument. Momentum mismeasurement due to multiple scattering requires significant track deflection. It can be induced just by one suitably large Coulomb scattering. This has low probability, besides, the scattering must take place in the center of magnet, otherwise the track quality would be poor. A large deflection is more likely to be a result of two or more scatterings. However, these scatterings must conspire to provide good track quality.

Clearly, good resolution is important for rejection of the muon scattering background. To demonstrate this, we have gradually raised the highest accepted momentum of secondary track. With a 32 GeV cut nothing is changed, with a 34 GeV cut there are 11 events in the mass plot with 5 in the region I, with a 36 GeV cut there are 145 events in the mass plot with 84 in the region I.

### Incorrect velocity spectrometer measurement

This scenario assumes basically correct measurement in the magnetic spectrometer, but severe mismeasurement in the velocity spectrometer. From the experience with the SELEX RICH we know that RICH response follows normal distribution few orders of magnitude (for the SELEX RICH tails outside of the  $\pm 5\sigma$  region constitute a fraction of  $4-8\times 10^{-5}$  [4]), thus we need to consider quite rare physical processes. Muon bremsstrahlung has been identified as one of the possible mechanisms. If a muon loses about 32% of its energy in the result of a bremsstrahlung, then the momentum measurement of the velocity spectrometer agrees with that of magnetic spectrometer. In that case the measured missing mass squared equals to

$$\text{MM}^2 = -(m_{\pi^+}^2 - m_{\mu^+}^2) \left( \frac{2E_{K^+}}{E_{\mu^+} + E'} - 1 \right) \approx -(m_{\pi^+}^2 - m_{\mu^+}^2) \frac{E_{K^+} - E_{\mu^+}}{E_{\mu^+}} \quad (1.11)$$

where  $E' = \sqrt{E_{\mu^+}^2 - m_{\mu^+}^2 + m_{\pi^+}^2}$ . Depending on the kaon and muon momenta, missing mass squared varies from  $-0.023$  to  $-0.002 \text{ GeV}^2$ , which is quite close to region I. Thus even gaussian resolution effects are sufficient to push events of this type into background for  $\pi^+\nu\bar{\nu}$ .

For the event to be reconstructible the bremsstrahlung must occur approximately between the last straw tube station DMS4 and the beginning of the pion RICH. More upstream or downstream bremsstrahlungs lead to high  $\chi^2$  when fitting for momentum in magnetic and velocity spectrometers respectively. Bremsstrahlung upstream of the DMS4 is rare any case, since that region is filled mostly with helium. For simulation of this process we have forced muon bremsstrahlung to take place just downstream of the DMS4. We have also requested photon energy to be at least 4 GeV. Probability of such a bremsstrahlung on 3 m of air and neon at atmospheric pressure is about  $4\cdot 10^{-7}$ .

Another possibility for a muon to lose significant fraction of energy is via  $\mu N$ -interaction. However, according to GEANT, probability of any  $\mu N$ -interaction on 3 m of air and neon at atmospheric pressure is about  $6 \cdot 10^{-8}$ . And usually an interaction produces more than one particle, so it is arguably easier to veto than a bremsstrahlung event. Consequently, we can safely neglect  $\mu N$ -interactions in this scenario.

We have simulated  $1 \cdot 10^6$   $K^+ \rightarrow \mu^+ \nu$  decays in fiducial decay volume, forced bremsstrahlung to take place if muon reached DMS4, performed kinematic reconstruction and applied standard selection criteria. The muon imitates a good pion in downstream magnetic and velocity spectrometers (that is, it passes reconstruction and track quality cuts, while the FVS, MVS, and  $MM^2$  cuts are not applied yet) in  $35 \cdot 10^3$  events. Missing mass squared for these events is shown in Fig. 1.4a. It is seen that sizable fraction of events (18%) falls into region I. These events are further suppressed by vetoing on the photon, which goes mostly into the FVS, and by vetoing on the muon in the MVS. Combining the  $K^+ \rightarrow \mu^+ \nu$  branching ratio, probability of bremsstrahlung and all efficiencies, we can express effective branching ratio as

$$\text{EBR} = 4.7 \cdot 10^{-8} \times \text{Efficiency}[\gamma] \times \text{Efficiency}[\text{MVS}] \quad (1.12)$$

For events which fall in the region I distributions on the photon energy and on the distance between the photon and the muon at the FVS are shown in Figs. 1.4b and 1.4c. Using standard veto inefficiency table, we obtain 50% probability that photon escapes detection. It is mainly caused by events where the photon is within 10 cm of the charged track. Fraction of events in which the photon misses the veto is much smaller: 0.4%. These are mainly the photons which escape the square SVS with a coverage of  $\pm 120$  cm. Fraction of photons going into the FVS hole is 0.05%.

Should it be necessary, we can significantly improve photon rejection in the FVS by requiring that a charged track shower shape is not compatible with a photon shower shape. Presumably this would make a small impact on the  $K^+ \rightarrow \pi^+ \nu \bar{\nu}$  efficiency. But even assuming perfect shower shape rejection, there remains 0.4% probability of photon missing veto aperture. In terms of effective branching ratio it means

$$\text{EBR} = 2 \cdot 10^{-10} \times \text{Efficiency}[\text{MVS}] \quad (1.13)$$

Thus we have found the background which actually requires the MVS. On the other hand, should we have  $10^{-4}$  muon rejection inefficiency in the MVS, there is almost no need in shower shape selection in the FVS.

In summary, we think the effective background ratio due to the  $K^+ \rightarrow \mu^+ \nu$  decay is less than  $1 \cdot 10^{-12}$ .

### 1.3.2 The $K^+ \rightarrow \pi^+ \pi^0$ background

The  $K^+ \rightarrow \pi^+ \pi^0$  decay is the second largest  $K^+$  decay with the branching ratio of 21.2%. Two ways to suppress this background are photon veto rejection and exploitation of the two-body kinematics.

In the P921 version of the CKM experiment this decay has been identified as the major source of background in the region I. Consequently, we have paid significant attention to the  $K^+ \rightarrow \pi^+ \pi^0$  decay.

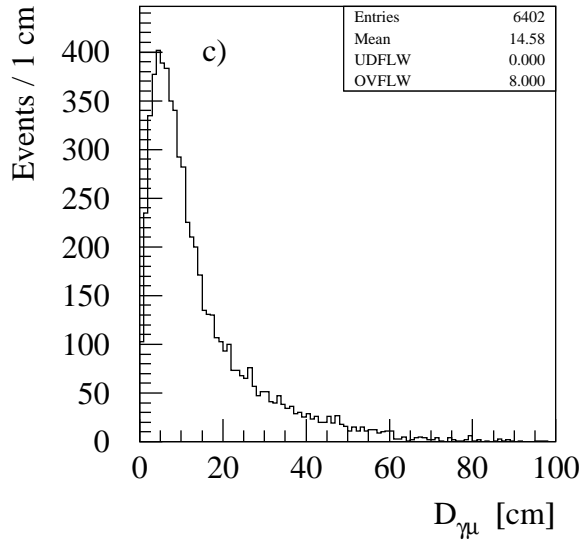
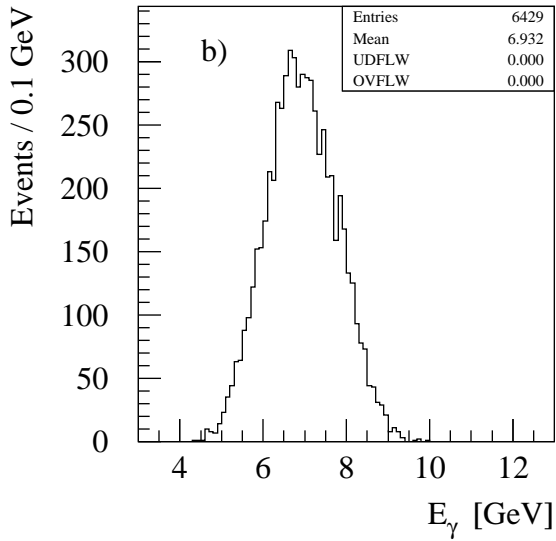
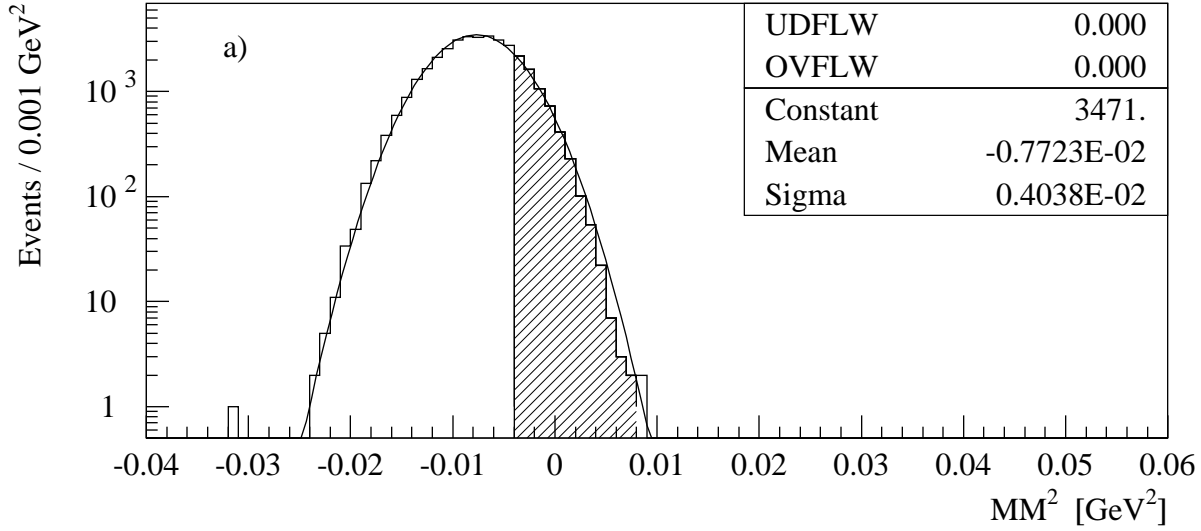


Figure 1.4: The  $K^+ \rightarrow \mu^+ \nu$  background, assuming that magnetic spectrometer measurement is correct, while muon bremsstrahlung corrupts velocity measurement. a) Reconstructed missing mass squared. Region I is shown hatched. b) Photon energy for region I events. c) Distance between photon and muon at the FVS.

Important feature of the P940 experiment, as compared to the P921, is different  $\pi^0$  energy spectrum. In the second version of the P921 proposal, only events with minimal  $\pi^0$  energy of 1 GeV can pass selection criteria on primary and secondary track momenta, while the typical  $\pi^0$  energy for passed events is 4.5 GeV. The P940 uses different charged tracks momentum regions, so that the minimal  $\pi^0$  energy is 7 GeV, while the typical one is 23 GeV. Thus it is easier to reject photons in the P940.

### Photon veto rejection

To estimate the  $\pi^0$  rejection we have simulated  $K^+ \rightarrow \pi^+\pi^0$  decays in fiducial decay region and applied all  $\pi^+\nu\bar{\nu}$  charged tracks selection cuts, except the cut on missing mass squared. Then we have determined the detector each photon goes into (if any), and, using listed in Table 1.1 photon veto inefficiencies, calculated the probability that both photons from the  $\pi^0$  decay escape vetoing.

The simulation shows that about 40% of all photons hit the VVS and about 58% hit the FVS. In 82% of the events at least one photon goes into the FVS. The  $\pi^0$  inefficiency, as a function of the decay vertex  $Z$ -coordinate, is shown in Fig. 1.5. It is rather uniform, thus demonstrating that chosen veto geometry is a reasonable first approximation. Integrated  $\pi^0$  veto inefficiency for the  $K^+ \rightarrow \pi^+\pi^0$  decays is  $1.0 \cdot 10^{-7}$ . Contributions of different event topologies to the inefficiency are listed in Table 1.3.

### Kinematic rejection

To estimate kinematic rejection we have allowed multiple scattering and elastic hadron scattering to occur. However, hadron scatterings have been limited only to the vacuum windows and DMS straw tubes. Hadron cross sections and interactions have been played by GEANT FLUKA. Photons from the  $\pi^0$  decay have not been traced.

Fraction of events which pass all selection cuts, except the cut on the missing mass squared, is 26.3% for region I and, because of shorter decay base, a lower number of 21.8% for region II. Probability that reconstructed missing mass squared falls into selected region is  $6.0 \cdot 10^{-5}$  for region I and  $1.2 \cdot 10^{-5}$  for region II. Obtained with the region I cuts missing mass squared distribution, as well as backgrounds in both regions, are shown in Fig. 1.6. For missing mass squared resolution we find  $\sigma = 1.8 \cdot 10^{-3} \text{ GeV}^2$  in a gaussian approximation.

It is interesting to note that none of the events with elastics hadron scatterings in the vacuum window and 5 events with hadron scatterings in the first DMS station have entered the missing mass squared plot. None of these has fallen into any selected region. This is different from the P921, where elastic hadron scatterings have been responsible for noticeable fraction of background. Continuing comparison with the P921, we find that region I missing mass squared rejection in the P940 is a factor of 3 worse than in the P921:  $6.0 \cdot 10^{-5}$  versus  $\approx 2 \cdot 10^{-5}$ .

### Overall rejection

When calculating the overall rejection inefficiency we use average values for acceptance, missing mass rejection and photon veto rejection. At present level of studies this is an

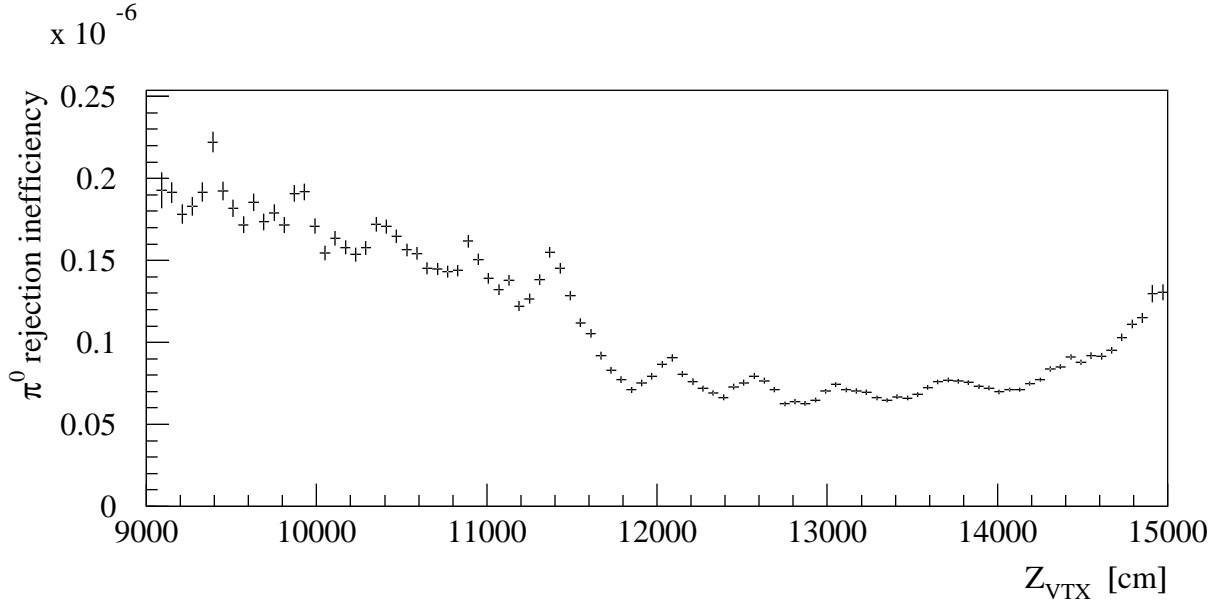


Figure 1.5: Inefficiency of the  $\pi^0$  vetoing in the  $K^+ \rightarrow \pi^+\pi^0$  decay as a function of vertex  $Z$  coordinate.

Contribution [%]	High Energy $\gamma$	Low Energy $\gamma$
21.9	VVS	Side Gap
21.5	VVS	VVS
14.1	VVS	Beam Hole
13.8	FVS	Beam Hole
10.5	FVS	Side Gap
7.1	FVS	VVS
4.5	VVS	Near $\pi^+$
2.6	FVS	Near $\pi^+$
2.4	Beam Hole	FVS
0.6	SVS	Beam Hole
0.3	SVS	Side Gap
$\Sigma < 1$	O T H E R	C A S E S

Table 1.3: Relative contributions to  $\pi^0$  inefficiency in the  $K^+ \rightarrow \pi^+\pi^0$  decay.

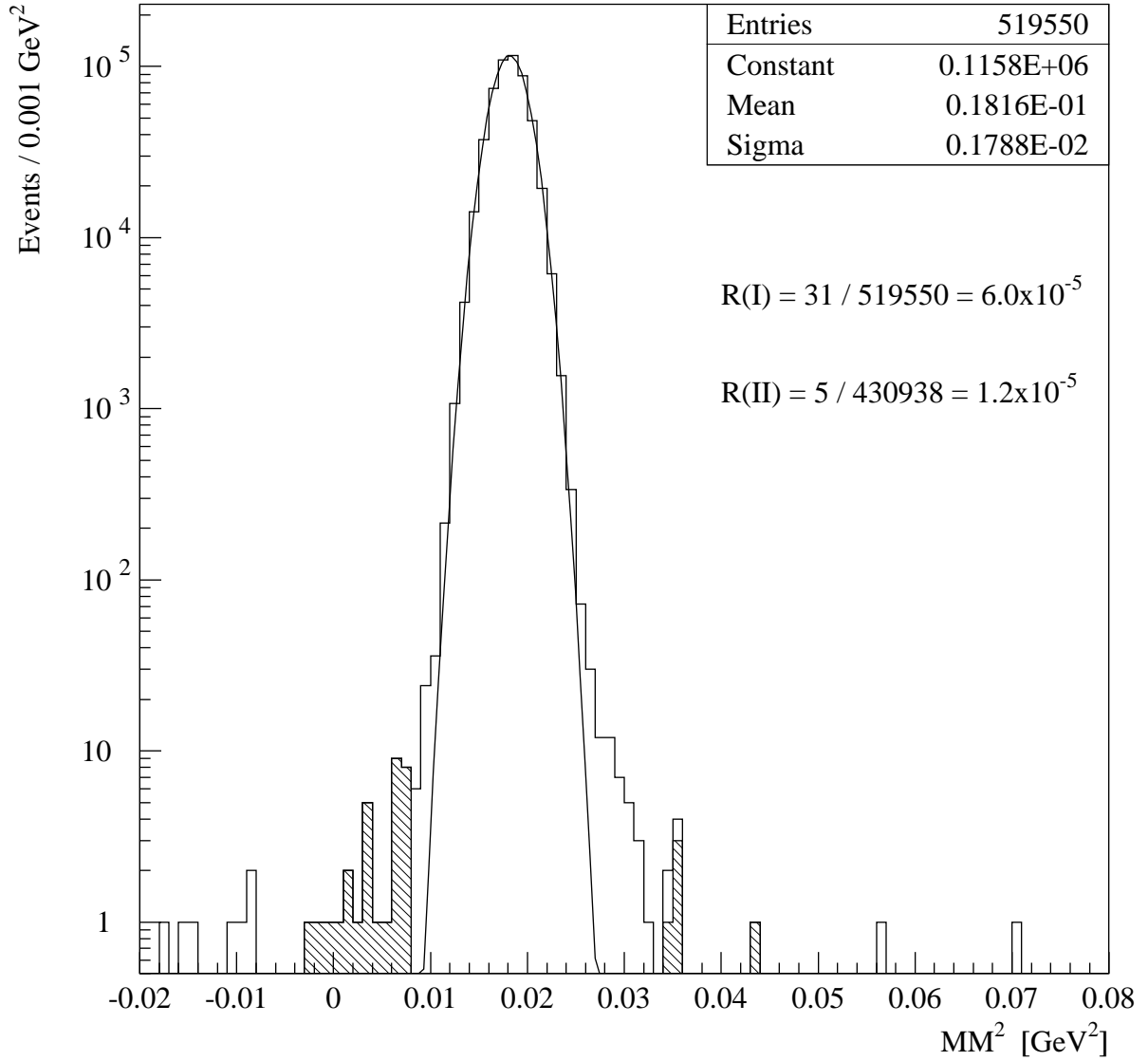


Figure 1.6: Missing mass squared distribution in the  $K^+ \rightarrow \pi^+\pi^0$  decay for events which pass all region I selection criteria, except the missing mass squared cut. Backgrounds in regions I and II are shown hatched. Note that region II has shorter decay base.

admissible approximation. Combining the  $K^+ \rightarrow \pi^+\pi^0$  branching ratio and all efficiency factors, we arrive at

$$\text{EBR(I)} = \frac{0.2116 \times 0.263 \times 6.0 \cdot 10^{-5} \times 1.0 \cdot 10^{-7}}{0.035} = 9.5 \times 10^{-12} \quad (1.14)$$

$$\text{EBR(II)} = \frac{0.2116 \times 0.218 \times 1.2 \cdot 10^{-5} \times 1.0 \cdot 10^{-7}}{0.050} = 1.1 \times 10^{-12} \quad (1.15)$$

## Caveats

The study presented is not comprehensive. We have ignored  $\pi^0$  Dalitz decays and photon conversions in the DMS straw tubes. As we have found in the P921 studies, these processes contribute only a small fraction to the total  $K^+ \rightarrow \pi^+\pi^0$  background. The same should be true for the P940 as well.

Another factor which may affect the  $K^+ \rightarrow \pi^+\pi^0$  background and which has been absent in the P921 geometry is the beam pipe. It happens once in a while that a photon hits the beam pipe, which is assumed to be 3 mm thick. Since the angle between photon direction and beam pipe directions is small, the photon travels large distance in the pipe substance and practically always starts showering. Thus some part of the photon energy is lost in the material of the pipe, while the rest is usually distributed over large area of the FVS, SVS, and sometimes VVS modules. Such events can be vetoed using the total energy deposits in the FVS and other photon vetoes. We have come to preliminary conclusion that beam pipe conversions present no problem, and even may help to veto events with photons going into the FVS hole. However, we find it difficult to quantitatively estimate the background until detailed understanding of rates and thresholds in every photon veto channel is developed.

### 1.3.3 The $K^+ \rightarrow \pi^+\pi^0\gamma$ background

In the limit of very low photon energies the  $K^+ \rightarrow \pi^+\pi^0\gamma$  decay is indistinguishable from the  $K^+ \rightarrow \pi^+\pi^0$  decay (infrared divergence). When the photon energy is required to exceed non-zero threshold (in the kaon rest frame), the decay becomes well defined. When the photon energy is small, it still looks like a  $K^+ \rightarrow \pi^+\pi^0$  decay. In particular, missing mass, which in this decay is  $\pi^0\gamma$  effective mass, is still very close to the  $\pi^0$  mass. As the photon energy raises, missing mass raises as well, and the two-body kinematic rejection becomes less efficient. However, decay branching ratio for that region of phase space goes down. Besides, as the photon energy in kaon rest frame raises, it on the average raises in the laboratory frame as well, thus making photon rejection more efficient.

To simulate the decay it is necessary first to select phase space region. We have chosen part of phase space with  $\pi^0\gamma$  effective mass corresponding to  $\pi^+\nu\bar{\nu}$  region II. Thus there is no kinematic rejection for that phase space region, and all the rejection comes from photon veto only.

## Matrix element and branching ratio

Theory summary of the  $K^+ \rightarrow \pi^+\pi^0\gamma$  decay and specific expressions for its matrix element can be found, for example, in [5, 6]. Two basic mechanisms contributing to the decay are

inner (or internal) bremsstrahlung (IB) and direct emission (DE). Theoretical description of the IB component is fully developed, and has been found to agree with experimental measurements. Theoretical description of the DE component contains two (electric and magnetic) amplitudes, which have to be determined experimentally. In the most precise up to date measurement [6] the DE contribution has been determined with about 20% accuracy. Also it has been found that interference of the two amplitudes is consistent with zero, and contributes to the branching ratio no more than few percent of IB.

Branching ratio as a function of the missing mass squared has been calculated by MC integration and is shown in Fig. 1.7. For decays which fall in the region II, which is shown hatched, branching ratio totals to  $2.4 \cdot 10^{-4}$ . DE contribution, shown by dashed line, is clearly small in the region II.

### Photon veto rejection

We simulate  $K^+ \rightarrow \pi^+\pi^0\gamma$  decays with all GEANT processes turned off, except for the multiple scattering. Fraction events which pass standard reconstruction and selection procedure is 28.9% (small technical point: to avoid finite resolution effects we apply selection on the true value of the missing mass squared, not the reconstructed one). The only other rejection of this decay comes from the photon veto. It has been determined with the standard photon veto inefficiency table and found to be  $3.2 \cdot 10^{-9}$ . Veto inefficiency for photons from the  $\pi^0$  decay is  $1.4 \cdot 10^{-7}$ , which is higher compared to  $1.0 \cdot 10^{-7}$  in the  $K^+ \rightarrow \pi^+\pi^0$  decay. This is not unexpected because of lower  $\pi^0$  average energy. Veto inefficiency for odd (internal bremsstrahlung) photon is 0.028. Energy of the bremsstrahlung photon and distance between it and the  $\pi^+$  at the FVS are shown in Fig. 1.8. It is worth noticing that when the  $\pi^0\gamma$  effective mass is not close to the  $\pi^0$  mass, as in the phase space region being considered, neither the photon energy is low, nor the photon is emitted in the  $\pi^+$  direction. As seen from number of events in plots in Fig. 1.8, only a little more than a half of bremsstrahlung photons reach the FVS. Combining the decay branching ratio for the chosen phase space region, kinematic reconstruction efficiencies and photon veto rejection, we arrive at

$$\text{EBR} = \frac{2.4 \cdot 10^{-4} \times 0.289 \times 3.2 \cdot 10^{-9}}{0.050} = 4.4 \times 10^{-12} \quad (1.16)$$

### Caveats

We have not investigated consequences of photon conversions in the beam pipe. We expect them to be of similar effect as in the  $K^+ \rightarrow \pi^+\pi^0$  decay.

Though the obtained estimate of the  $K^+ \rightarrow \pi^+\pi^0\gamma$  background is quite reliable, it refers only to a part of the phase space. Decays with higher  $\pi^0\gamma$  effective masses clearly contribute little. Decays with  $\pi^0\gamma$  effective masses in the region from  $m_{\pi^0}^2$  to  $0.032 \text{ GeV}^2$  require combined study of photon veto rejection and kinematic rejection. However, as the first estimate we can assume some intermediate value between the two extreme cases: only kinematic rejection ( $1.1 \cdot 10^{-12}$ ) for pure  $K^+ \rightarrow \pi^+\pi^0$  decay, and no kinematic rejection at all ( $4.4 \cdot 10^{-12}$ ) for the chosen part of the phase space. Thus we can expect the contribution of the order of  $2.5 \cdot 10^{-12}$ . It is certainly under control, since we can always raise a little the lower boundary of the missing mass squared cut, simultaneously reducing kinematic rejection inefficiency, photon veto inefficiency and relevant  $K^+ \rightarrow \pi^+\pi^0\gamma$  branching ratio.

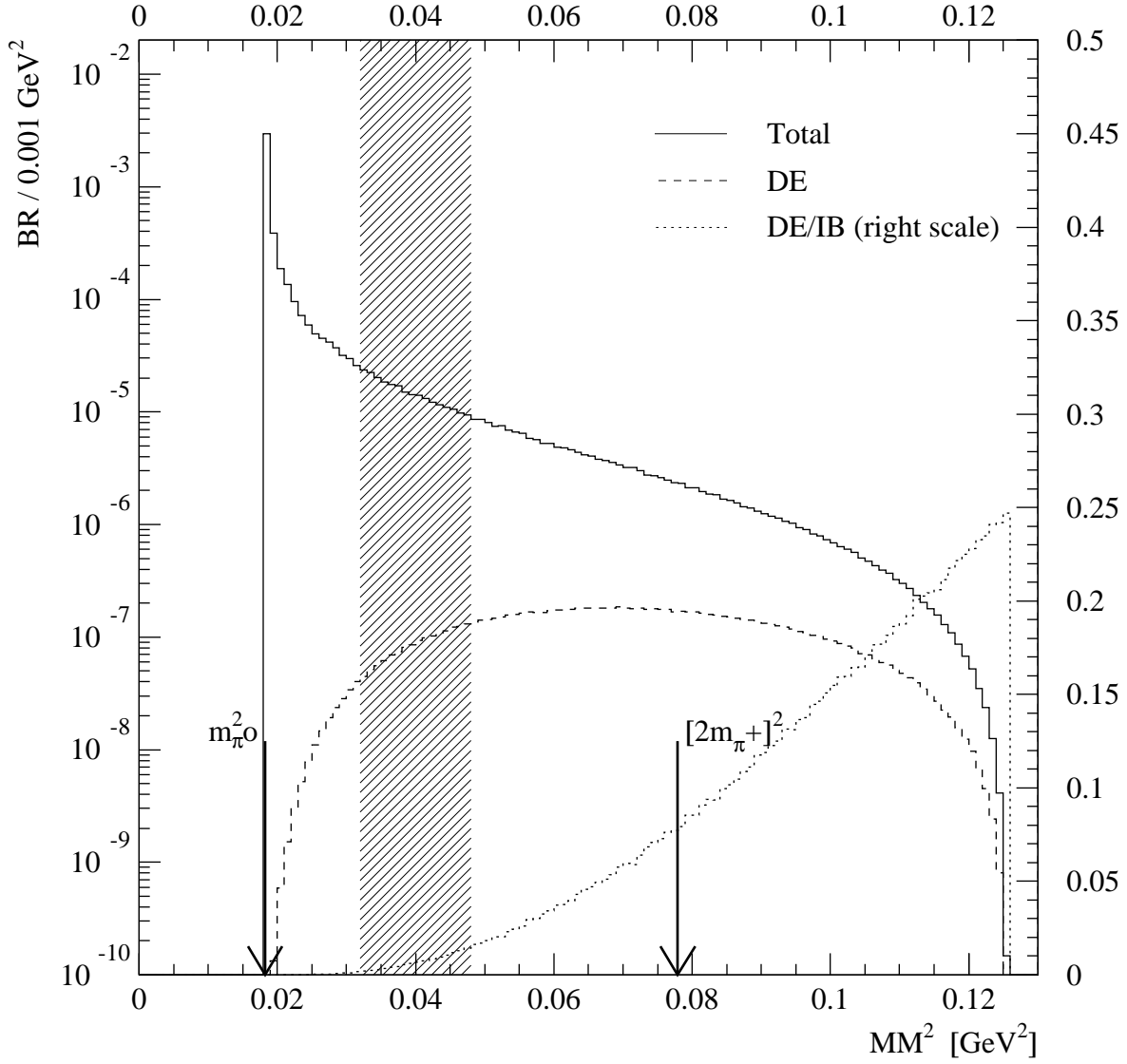


Figure 1.7: Branching ratio of the  $K^+ \rightarrow \pi^+ \pi^0 \gamma$  decay as a function of missing mass squared. Nominal  $K^+ \rightarrow \pi^+ \nu \bar{\nu}$  region II is shown hatched.

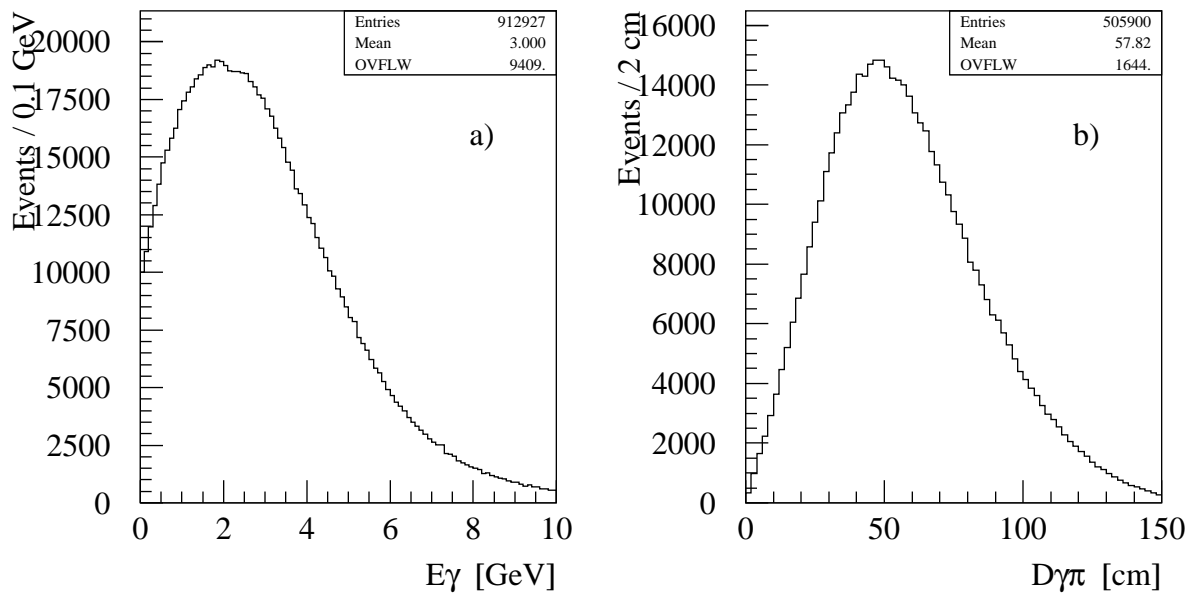


Figure 1.8: Bremsstrahlung photon properties in the  $K^+ \rightarrow \pi^+ \pi^0 \gamma$  decay: a) Energy in the laboratory frame; b) Distance to the  $\pi^+$  at the FVS.

### 1.3.4 The $K^+ \rightarrow \pi^+\pi^-e^+\nu$ background

Branching ratio of the  $K^+ \rightarrow \pi^+\pi^-e^+\nu$  decay is  $(3.91 \pm 0.17) \times 10^{-5}$ , which is quite low absolute value, but quite high compared to that of  $K^+ \rightarrow \pi^+\nu\bar{\nu}$ . Matrix element of this four-body decay is quite complicated [5], that is why we have started analysis with uniform over the phase space distribution. Before proceeding with detailed analysis, we would like to emphasize an importance of this decay for region II: it limits the missing mass squared from above, decreases the available decays base, and also leads to higher global veto inefficiency.

#### Efficiency of the $\pi^+$ selection

Since  $K^+ \rightarrow \pi^+\pi^-e^+\nu$  is a four-body decay, there is no kinematic rejection. However, not every point of the phase space can meet  $K^+ \rightarrow \pi^+\nu\bar{\nu}$  selection criteria and produce background candidates. To estimate fraction of the selected events, we have applied standard selection procedure to  $K^+$  and  $\pi^+$  only, "forgetting" for the moment about  $\pi^-$  and  $e^+$ . Missing mass (same as effective  $\pi^-e^+\nu$  mass) squared distribution for events which pass all the cuts, except the cut on the  $MM^2$  itself (29.9%), is shown in Fig. 1.9a. Fraction of the events which fall in the region II is 4.2%. Combining the  $K^+ \rightarrow \pi^+\pi^-e^+\nu$  branching ratio and  $\pi^+$  selection efficiencies, we can express overall effective branching ratio as

$$\text{EBR} = 9.8 \cdot 10^{-6} \times \text{Efficiency}[e^+] \times \text{Efficiency}[\pi^-] \quad (1.17)$$

Consequently, to keep this background to about 10% of the signal, combined  $e^+$  and  $\pi^-$  rejection inefficiency must be on the  $10^{-6}$  level.

#### Inefficiency of the $e^+$ rejection

Rejection of the  $e^+$  can be made by vetoing on extra hits in photon veto detectors, pion RICH, and DMS straw tubes. First we have studied the electron rejection in photon detectors. We have started with the same inefficiency rejection for electrons as for photons. But soon it has become clear that overall electron rejection inefficiency is quite large, so that there is no practical sense in accounting for very low inefficiencies. That is why we have simplified inefficiencies in Table 1.1 by setting to zero all numbers which are less than one. We have obtained a value of 10.4% for electron rejection inefficiency by photon veto detectors. It looks rather high. It should not be surprising, though, because an electron in a four-body decay can be of arbitrary low energy and go in any direction. Electron momentum distribution for kinematically selected in region II events is shown in Fig. 1.9b. Also, some "medium-energy" electrons miss veto due to deflection in the magnet, a mechanism impossible for photons.

Another device capable of vetoing  $e^+$  is the pion RICH. However, it can not improve rejection, already achieved with photon veto detectors. This is because all the electrons which are within the RICH acceptance hit either the FVS or SVS, and have sufficiently high energy to be vetoed at least at  $10^{-5}$  level.

The only remaining tool to further suppress electrons is the DMS straw tubes. Quite often electron does not produce a track or even a reconstructible segment in the DMS, consequently, we need to veto on extra hits in the DMS tubes. If we require that no tube is hit, the  $e^+$  rejection inefficiency is lowed to 2.2%. It is certainly an over-optimistic assumption that we can veto on just 6 or 8 extra hits in one DMS station without severe penalty in global

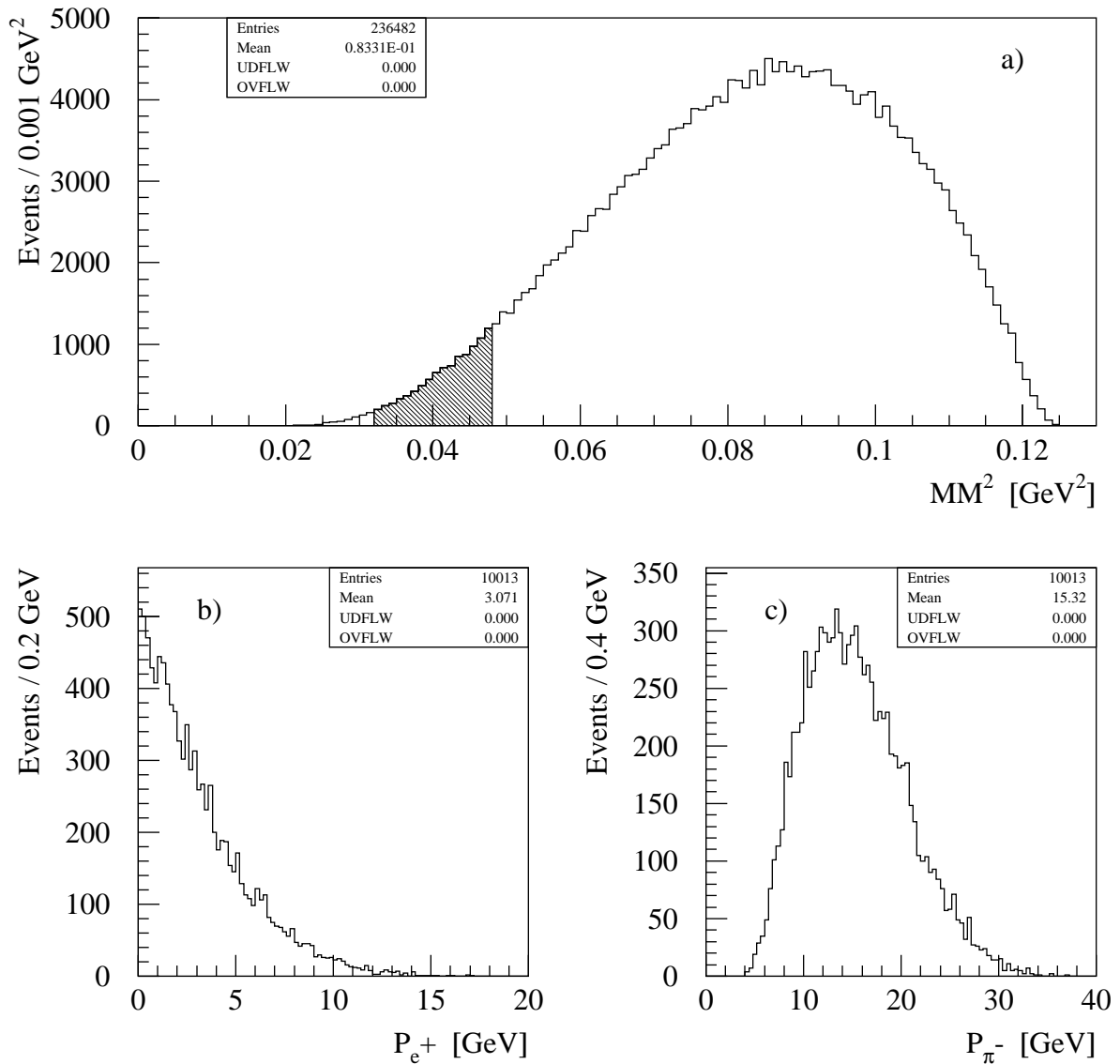


Figure 1.9: Properties of the  $K^+ \rightarrow \pi^+ \pi^- e^+ \nu$  decay.

- a) Missing mass squared distribution for events which pass all the region II selection criteria, except the cut on the missing mass.
- b) Electron momentum for selected region II events.
- c) Negative pion momentum for selected region II events.

inefficiency. But as we are about to show, the  $\pi^-$  rejection also requires vetoing on extra DMS hits, and ultimately the background events are those in which the electron just misses the veto.

It is important to realize that the 2.2% inefficiency can not be made much lower. By lowering a threshold in photon vetoes it is possible to achieve a factor of few improvement, but not orders of magnitude. Thus for negative pions we need to obtain a rejection inefficiency on the level of  $10^{-4}$  or better.

### Inefficiency of the $\pi^-$ rejection

A  $10^{-4}$  number, mentioned in previous subsection, is an "effective" required  $\pi^-$  rejection inefficiency. However, we do not assume any factorization between the  $e^+$  and  $\pi^-$  rejections, but perform the studies on event by event basis. We have generated a large number of  $K^+ \rightarrow \pi^+\pi^-e^+\nu$  events, equivalent to  $79 \cdot 10^6$   $K^+$  decays in fiducial volume. It follows that 1 event of this data set corresponds to an effective background ratio of  $9.8 \cdot 10^{-12}$ .

First we are going to demonstrate that the  $K^+ \rightarrow \pi^+\pi^-e^+\nu$  background can be controlled with a very conservative set of cuts. Then we take a more detailed look on the cuts employed, and discuss possibilities of increasing  $K^+ \rightarrow \pi^+\nu\bar{\nu}$  acceptance by extending the region II definition.

Most of the  $\pi^-$  miss the VVS. However, if a  $\pi^-$  does hit the VVS, we can safely assume that it is vetoed. As seen from Fig. 1.9c, minimal  $\pi^-$  momentum is 4 GeV. Any VVS inefficiency to such pions is much less than required pion rejection inefficiency.

We require that there is no activity in the FVS and SVS, except for the  $\pi^+$  signal. Of course, there is a possibility that a  $\pi^-$  hits the FVS near the  $\pi^+$  and thus escapes rejection. We assume perfect  $\pi^-$  rejection if two pions are at least 20 cm apart and no rejection whatsoever if they are closer, independently of whether any of pions showers or deposits a MIP.

We use the DMS straw tubes as a veto, requiring that there are no more than 18 planes with additional hits, i.e. excluding those produced by the  $\pi^+$ , but including those produced by the  $e^+$ . Given the 25 ns maximal drift time, we do not expect large  $K^+ \rightarrow \pi^+\nu\bar{\nu}$  inefficiencies caused by close in time charged particles, while 18 seems sufficiently high number to avoid accidental losses due to other miscellaneous reasons.

Four events satisfy all these cuts and cuts on the  $e^+$ , described in the previous subsection. In two of them the  $\pi^-$  is close to  $\pi^+$ , in the other two the  $\pi^-$  goes into the FVS beam hole. This reflects general feature of remaining background: the  $\pi^-$  always goes into forward direction, and there exist only two possibilities to escape rejection: pass through the beam hole or merge with  $\pi^+$ . Another feature of remaining background, imposed by the extra DMS hits cut, is that the  $\pi^-$  is quite close to the beam axis. Thus if the  $\pi^-$  momentum is above the Cherenkov radiation threshold of 12 GeV in the RICH, some fraction of light is absorbed by the beam pipe. That makes it difficult to describe RICH response accurately in the employed framework of fast ray trace simulation.

Some properties of the four background events are shown in Table 1.4. Taking into account that the beam pipe can not intercept more than half of the emitted light, we estimate around 1.5–3 photoelectrons in the first event, 0 in the second, 3–4 in the third, 6–8 in the

forth. With the help of the RICH we can definitely reject one event, and probably two. For final background estimate we assume that on the average the pion RICH rejects 1.5 events out of 4. That corresponds to an effective branching ratio

$$\text{EBR} = 25 \times 10^{-12} \quad (1.18)$$

Now let us take a more careful look at the cuts employed. Distribution on the total number of extra hits in the DMS straw tubes prior to cut on that variable is shown in Fig. 1.10. The same distribution for events with  $P_{\pi^-} < 14 \text{ GeV}$  (which can not be efficiently rejected by the pion RICH) is shown hatched. We see that the cut value of 18 is more or less reasonable. A somewhat higher value results in much higher background, a more aggressive cut could kill all the background events, however, the price in terms of global inefficiency could be unacceptably high.

Positions of the  $\pi^-$  at the FVS are shown in Fig. 1.11, with distance to the  $\pi^+$  being encoded by marker type. It is seen that  $\pi^-$  hits occupy only a part of the FVS, mostly to the right of the beam hole. This is understandable, because requirement on the number of traversed DMS planes ensures that the track passes in the vicinity of the beam axis, while the magnet smears and shifts the distribution. If the  $\pi^-$  does not go into the beam hole, a MIP veto threshold for the indicated part of the FVS seems the most reliable way to reject the background, though the MVS can be used as well. It is also worth noticing that, because of kinematics and applied selection criteria, the  $\pi^-$  can overlap with the  $\pi^+$  only in a very limited region of the FVS. We can suppress these events limiting region II acceptance by requirement that the  $\pi^+$  hits the FVS sufficiently far from the possible overlap region. So we have some tools to control the  $K^+ \rightarrow \pi^+\pi^-e^+\nu$  background in reserve.

Now we briefly investigate possibility to raise  $K^+ \rightarrow \pi^+\nu\bar{\nu}$  acceptance by extending our region II definition. Should it be feasible to use higher missing mass squared, up to the value of  $0.068 \text{ GeV}^2$ , set by the  $K^+ \rightarrow \pi^+\pi^+\pi^-$  decay, and should it be possible to use all the decay base up to 15000 cm, the region II acceptance would raise from 5.0% to 11.7%. Because of change in acceptance the single event sensitivity is also changed. In the plots which follow 1 event corresponds to an effective background ratio of  $4.2 \cdot 10^{-12}$ .

The scatter plot of reconstructed missing mass squared versus decay vertex  $Z$ -coordinate for the selected with standard procedure  $K^+ \rightarrow \pi^+\pi^-e^+\nu$  decay events is shown in Fig. 1.12. Standard and extended region II definitions are shown by dotted lines. Events with  $P_{\pi^-} < 14 \text{ GeV}$  and total number of DMS planes with extra hits no more than 12 are indicated by black triangles. We see that the black triangles occupy most of the region II extension. Hit positions of the  $\pi^-$  at the FVS for events in extended region II are shown in Fig. 1.13. Again, no more than 12 extra hit DMS planes are allowed. Comparing with Fig. 1.11, we see that hits occupy larger area, the same being true for those  $\pi^-$  which are close to the  $\pi^+$  as well. Also, much more events go into the beam hole. From these figures we conclude that it is not possible to increase  $K^+ \rightarrow \pi^+\nu\bar{\nu}$  acceptance by a factor of 2 or even by 50%, simultaneously keeping the  $K^+ \rightarrow \pi^+\pi^-e^+\nu$  background and global inefficiency at low levels. But a 25% improvement may be achievable.

## Concluding remarks

At our present level of understanding we consider the  $K^+ \rightarrow \pi^+\pi^-e^+\nu$  decay as the most troublesome. We do not pretend to have studied it completely. Matrix element has not been

Event	pn	dprcn	lfvhn	dist
228929	13.1947	1728.42	0	12.7924
248176	8.13264	1849.27	0	16.3314
292782	15.3016	983.524	1	28.7396
364610	20.0866	1140.53	1	44.2546

Table 1.4: Some properties of four  $K^+ \rightarrow \pi^+\pi^-e^+\nu$  background events:

pn —  $\pi^-$  momentum [GeV];

dprcn — path in pion RICH radiator [cm];

lfvhn — flag whether  $\pi^-$  goes into FVS beam hole;

dist — distance to  $\pi^+$  at the FVS [cm].

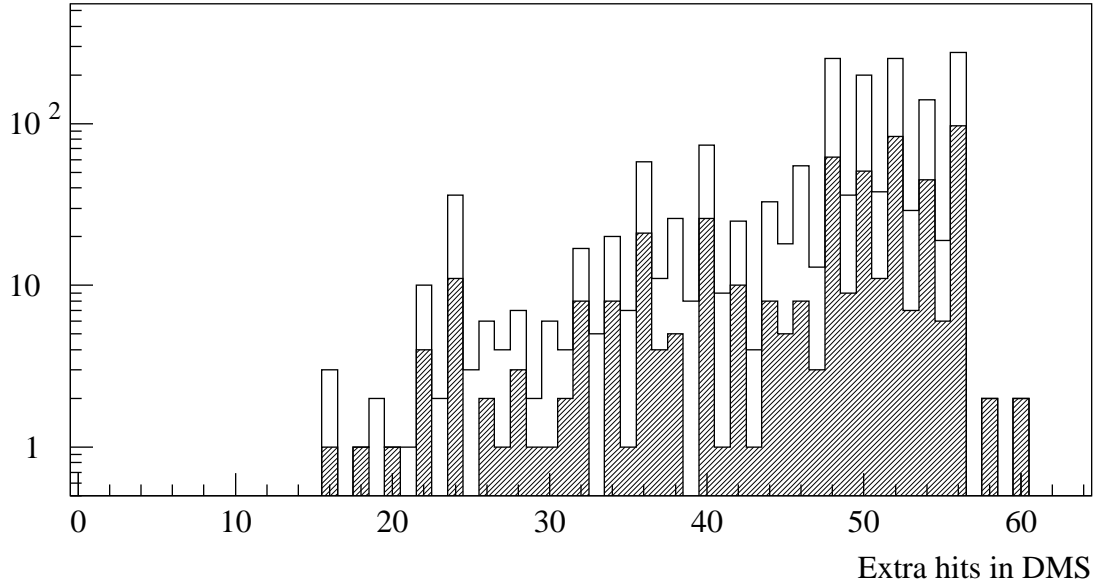


Figure 1.10: Number of extra hits in the DMS straw tubes. All region II cuts and  $K^+ \rightarrow \pi^+\pi^-e^+\nu$  suppression cuts are applied. Hatched distribution corresponds to events with  $P_{\pi^-} < 14$  GeV.

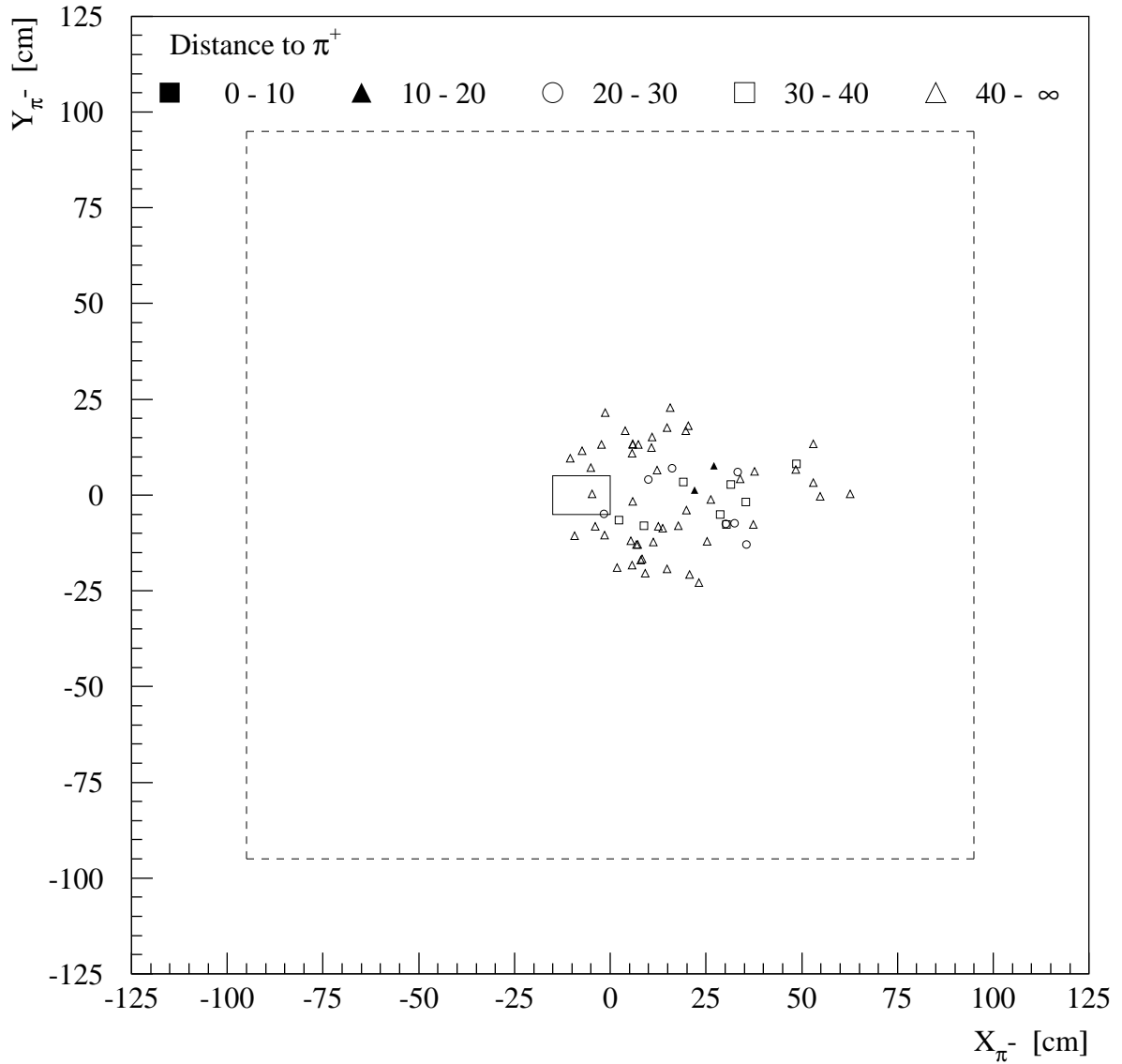


Figure 1.11: Position of the  $\pi^-$  at the FVS. All region II cuts and  $K^+ \rightarrow \pi^+ \pi^- e^+ \nu$  suppression cuts are applied. Dashed line shows FVS size, the rest is covered by the SVS. Rectangle in the center shows the beam hole. Distance to the  $\pi^+$  is encoded by marker type.

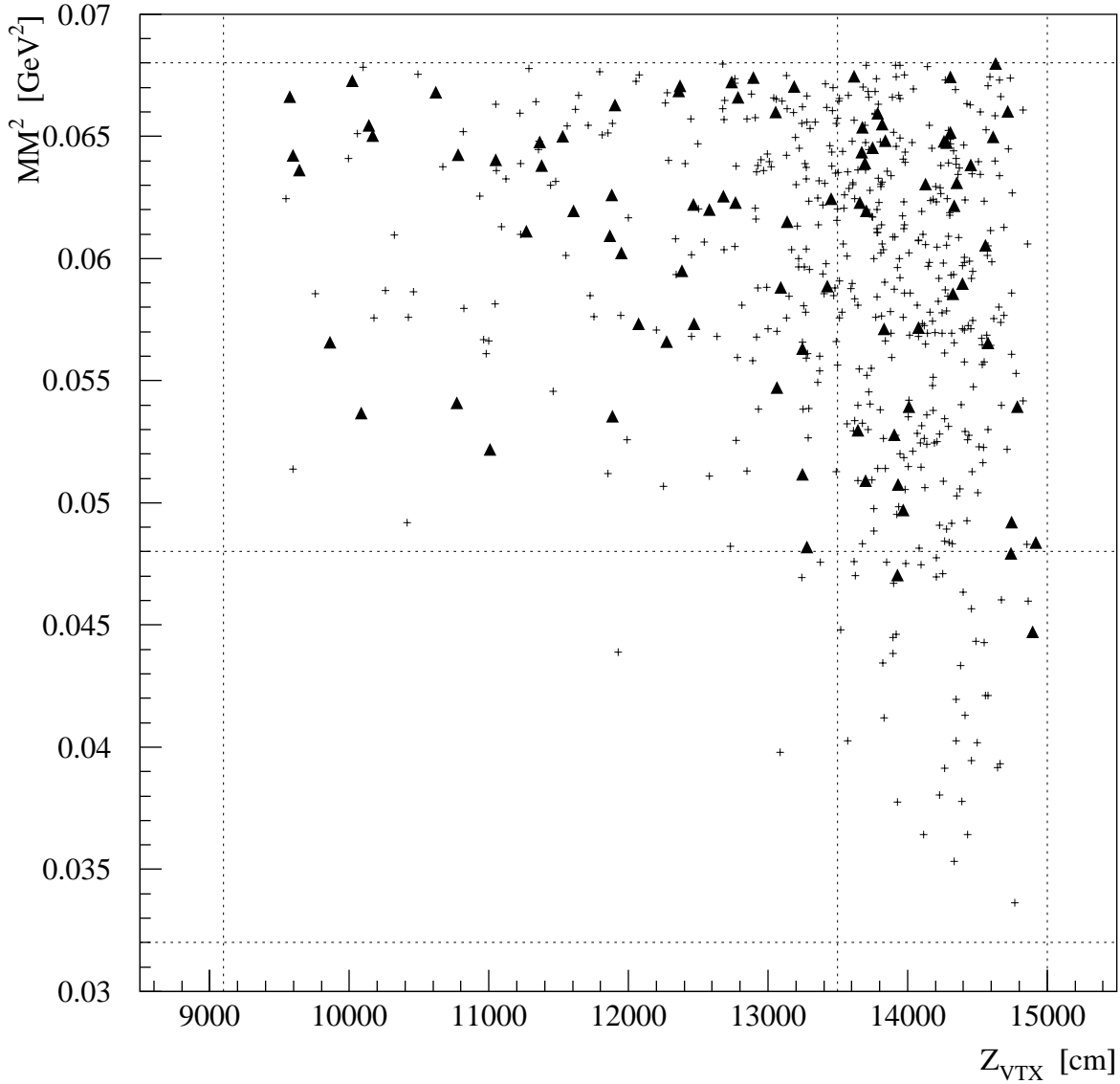


Figure 1.12: The  $K^+ \rightarrow \pi^+ \pi^- e^+ \nu$  background in extended region II. Reconstructed missing mass squared versus decay  $Z$ -vertex. Dotted lines show standard and extended region II definitions. Markers show background events which pass all the standard selection criteria, with black triangles showing events satisfying more stringent criteria: no more than 12 DMS planes with extra hits and  $P_{\pi^-} < 14$  GeV.

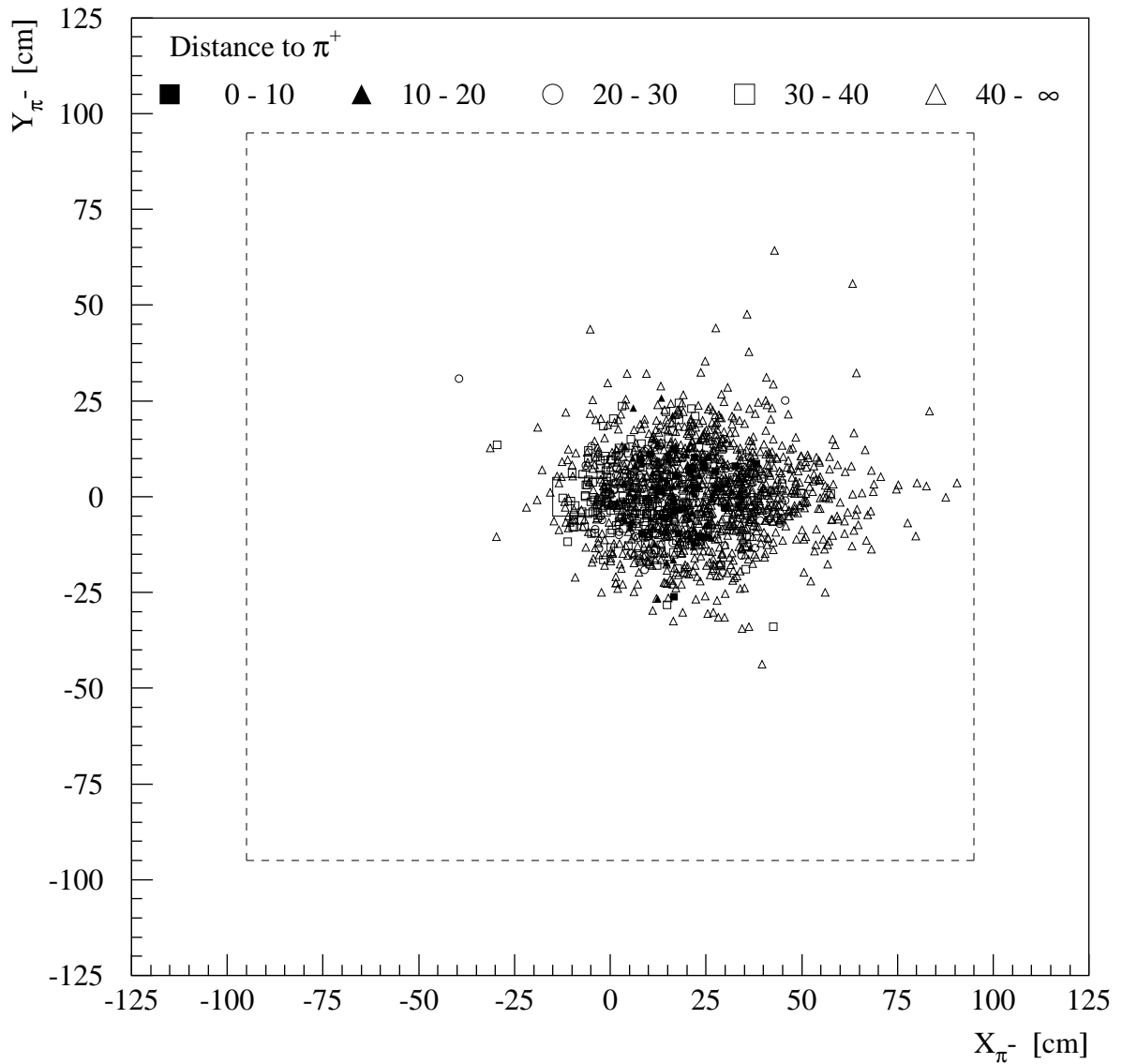


Figure 1.13: Position of the  $\pi^-$  at the FVS with region II extended. All region II cuts and  $K^+ \rightarrow \pi^+\pi^-e^+\nu$  suppression cuts are applied, with maximal number of DMS planes with extra hits being set to 12. Dashed line shows FVS size, the rest is covered by the SVS. Rectangle in the center shows the beam hole. Distance to the  $\pi^+$  is encoded by marker type.

taken into account. Events where the  $\pi^-$  decays or interacts in the beam pipe have been studied rather superficially, with the preliminary conclusion that these do not create new problems. For the selected region II definition with 5% acceptance the background is under control. It seems likely that cuts can be optimized to increase the acceptance. However, it is a difficult multiparameter problem, in which background, acceptance, and global inefficiency in the DMS, pion RICH and FVS are all interwoven. There is even a possibility of optimizing the detector geometry by moving the straw tubes in the first two DMS stations closer to the beam.

### 1.3.5 The $K^+ \rightarrow \pi^+\pi^-\mu^+\nu$ background

Branching ratio of this decay is  $(1.4 \pm 0.9) \times 10^{-5}$ . Missing mass squared lower threshold for this decay equals  $(m_{\pi^-} + m_{\mu^+})^2 = 0.060 \text{ GeV}^2$ . This is comfortably higher than the region II upper limit of  $0.048 \text{ GeV}^2$ . For a separation of  $0.012 \text{ GeV}^2$  we can expect kinematic rejection inefficiency similar to that of  $K^+ \rightarrow \pi^+\pi^0$  case, or of the order of  $6 \cdot 10^{-5}$ . Thus even very mild veto requirements on  $\mu^+$  and  $\pi^-$  make this background completely negligible.

We are going to argue further that the  $K^+ \rightarrow \pi^+\pi^-\mu^+\nu$  decay, should it be possible to extend the region II missing mass squared upper limit up to  $0.068 \text{ GeV}^2$ , still creates no problems. We follow the  $K^+ \rightarrow \pi^+\pi^-e^+\nu$  study by applying standard reconstruction and selection criteria to  $K^+$  and  $\pi^+$ , while "forgetting" about  $\mu^+$  and  $\pi^-$ . We also use all the available decay base for that calculation. Such an extended region II has an acceptance of 11.7%. Missing mass squared distribution, assuming uniform over the phase space matrix element, is shown in Fig. 1.14a. Fraction of events which go into mass plot is 25.6%, fraction of events in mass plot which fall into region II is 0.4%. Combining all the numbers, we can express the effective branching ratio as

$$\text{EBR} = 1.3 \cdot 10^{-7} \times \text{Efficiency}[\mu^+] \times \text{Efficiency}[\pi^-] \quad (1.19)$$

We show  $\mu^+$  and  $\pi^-$  momentum distributions for selected region II events in Figs. 1.14b and 1.14c. It is important that both distributions start from non-zero threshold, thus promising good rejection prospects. For example, even a very modest requirement that the muon hits no vacuum veto and less than 24 DMS planes provides a factor of 8 rejection. This alone, assuming similar  $\pi^-$  rejection, makes the  $K^+ \rightarrow \pi^+\pi^-\mu^+\nu$  background a factor of few smaller than the  $K^+ \rightarrow \pi^+\pi^-e^+\nu$  one. Considering that remaining muons almost always hit the FVS, and that each muon hit in the DMS improves the overall rejection, even an order of magnitude estimate for difference in backgrounds seems too conservative.

### 1.3.6 The $K^+ \rightarrow \pi^+\pi^+\pi^-$ background

Branching ratio of the  $K^+ \rightarrow \pi^+\pi^+\pi^-$  decay is 5.6%. The lowest possible missing mass squared in the decay is  $(2m_{\pi^\pm})^2 = 0.078 \text{ GeV}^2$ . This is substantially higher than our region II upper limit of  $0.048 \text{ GeV}^2$ . But even the extended up to  $0.068 \text{ GeV}^2$  region II should provide excellent rejection. For events with missing mass squared in the  $0.078\text{--}0.088 \text{ GeV}^2$  the resolution, in gaussian approximation, corresponds to  $\sigma = 0.9 \cdot 10^{-3} \text{ GeV}^2$ . In the simulation with multiple scattering allowed but hadron elastic disabled, we have obtained the kinematic rejection inefficiency of  $(2.6 \pm 1) \times 10^{-6}$ , which must be combined with 34% probability that an event passes all the selections to get to the mass plot. Thus we can express

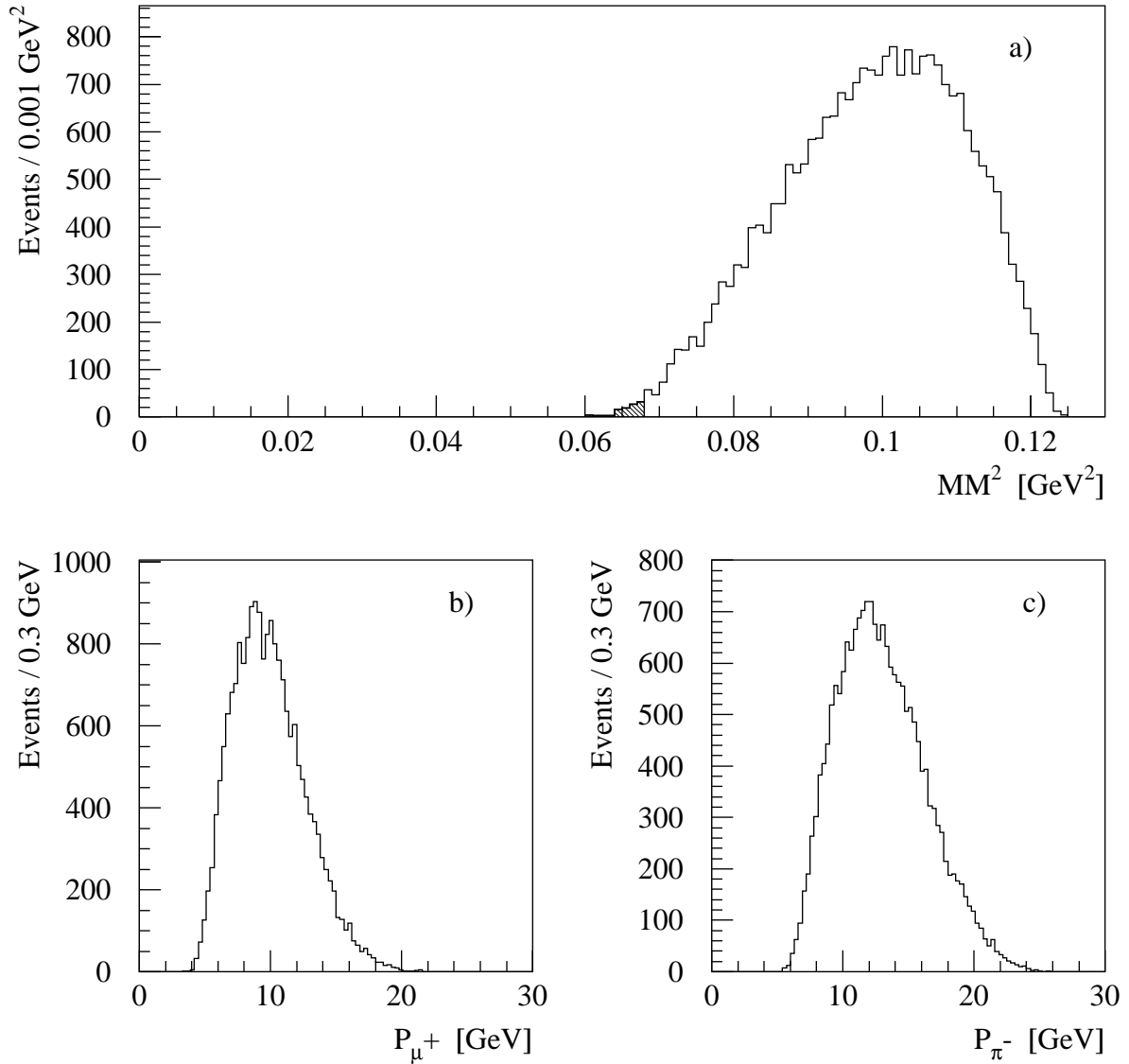


Figure 1.14: Properties of the  $K^+ \rightarrow \pi^+ \pi^- \mu^+ \nu$  decay.  
 a) Missing mass squared distribution for events which pass all the "extended" region II selection criteria, except the cut on the missing mass.  
 b) Muon momentum for selected region II events.  
 c) Negative pion momentum for selected region II events.

the effective background ratio as

$$\text{EBR} = 4.0 \cdot 10^{-7} \times \text{Efficiency}[\pi^+] \times \text{Efficiency}[\pi^-] \quad (1.20)$$

Pion momentum spectrum in the  $K^+ \rightarrow \pi^+\pi^+\pi^-$  decay starts from 5 GeV in the laboratory frame. For events with missing masses near the threshold minimal pion momentum is 6 GeV. Selection criteria, employed to veto  $\pi^-$  in the  $K^+ \rightarrow \pi^+\pi^-e^+\nu$  decay, are expected to be even more effective in rejecting pions in this decay. Thus the effective background ratio for the extended region II is likely to be below  $1 \cdot 10^{-12}$ .

### 1.3.7 Other kaon decay backgrounds

In this section we deal with decays which we consider harmless for a 100 event  $K^+\pi^+\nu\bar{\nu}$  measurement. For the purpose of background studies it is convenient to classify kaon decays on the type of heaviest positively charged  $K^+$  decay product, which will have to imitate pion.

Decays with an  $e^+$  as the heaviest positive  $K^+$  decay product are highly unlikely to be a source of any background. This is because any high energy electron produces maximal radius ring in the pion RICH and thus vetoed, because the  $e^+$  is absorbed in the FVS and thus has no way to imitate pion in the MVS, and because the  $K^+ \rightarrow e^+\nu$  decay has a small branching ratio of  $1.6 \cdot 10^{-5}$ , the  $K^+ \rightarrow \pi^0e^+\nu$  decay has an extra  $\pi^0$ , etc.

Decays with a  $\mu^+$  as the heaviest positive  $K^+$  decay product are more likely to be a source of background. In contrast to  $K^+ \rightarrow \mu^+\nu$ , no two-body kinematic constraint can be used to reject  $K^+ \rightarrow \mu^+X$  decays. However, the missing mass squared selection played a very limited role in the rejection of the  $K^+ \rightarrow \mu^+\nu$  background, while significant additional rejection factors are associated with other decays. The decay

$$K^+ \rightarrow \pi^0\mu^+\nu \quad (1.21)$$

has a branching ratio of 3.3% and two photons from the  $\pi^0$  decay. The decay

$$K^+ \rightarrow \mu^+\nu\gamma \quad (1.22)$$

coincides with  $K^+ \rightarrow \mu^+\nu$  in the low photon energy limit, while for photon energies above some threshold has a small branching ratio and an extra photon. Thus we conclude that all the  $\mu^+$  backgrounds are negligible.

Decays with a  $\pi^+$  as the heaviest positive  $K^+$  decay product are potentially the most dangerous. Most of them are considered in more detail below, except for few radiative decays which evidently present no problem.

#### The $K^+ \rightarrow \pi^+\pi^0\pi^0$ background

Branching ratio of the  $K^+ \rightarrow \pi^+\pi^0\pi^0$  decay is 1.73%. Missing mass squared lower threshold for this decay is  $(2m_{\pi^0})^2 = 0.073 \text{ GeV}^2$ , which is higher even then the "extended" region II. Besides, there is enormous photon rejection. Lab frame kinematics of this decay is such that each  $\pi^0$  has an energy of at least 4.5 GeV. Thus only the high energy photons should provide rejection inefficiency of the order of  $10^{-10}$ . In all probability this decay can not be a background to any point of the  $K^+ \rightarrow \pi^+\nu\bar{\nu}$  phase space.

### The $K^+ \rightarrow \pi^+ \gamma \gamma$ background

Thus far the  $K^+ \rightarrow \pi^+ \gamma \gamma$  decay has been measured in only one experiment [7]. In our previous proposal studies [3] we have concluded that corresponding background is far below the  $1 \cdot 10^{-12}$  level for region I in the P921 geometry. The same is expected to be true for P940 as well, since photon rejection in the P940 is similar.

The  $K^+ \rightarrow \pi^+ \gamma \gamma$  branching ratio for the region II is a factor of few higher than for the region I. Using the model dependent fit of pion momentum in this decay, performed in [7], we estimate the branching ratio in region II to be  $2 \cdot 10^{-8}$ . This corresponds to

$$\text{EBR(II)} = 1.2 \cdot 10^{-7} \times \text{Efficiency}[\gamma\gamma] \quad (1.23)$$

In the accepted events there is always one high energy photon, rejection inefficiency of which is  $1 \cdot 10^{-5}$  in the VVS and  $3 \cdot 10^{-6}$  in the FVS. It alone gives  $\text{EBR(II)} < 1 \cdot 10^{-12}$ . Thus we conclude that the background is far below  $1 \cdot 10^{-12}$  for region II as well as for region I.

### The $K^+ \rightarrow \pi^+ e^+ e^-$ background

Branching ratio of the  $K^+ \rightarrow \pi^+ e^+ e^-$  decay is  $2.88 \cdot 10^{-7}$ . In the latest measurement of that decay [8] its vector nature has been firmly established and its formfactor accurately determined. This allows us to compute branching ratios for arbitrary region in phase space. We have obtained a value of  $3.1 \cdot 10^{-8}$  for decays which fall in region I and  $5.4 \cdot 10^{-8}$  for region II. Event selection procedure guarantees that at least one of the electrons is of high energy (more than 3.5 GeV), thus providing rejection with better than  $10^{-5}$  inefficiency. So the background is far below  $1 \cdot 10^{-12}$ .

### The $K^+ \rightarrow \pi^+ \mu^+ \mu^-$ background

Branching ratio of the  $K^+ \rightarrow \pi^+ \mu^+ \mu^-$  decay is  $(8.1 \pm 1.4) \times 10^{-8}$ . Using the most precise measurement of this decay [9], we have estimated the fraction of decays which fall into extended region II to be about 1/3. Reconstruction efficiency is expected to be similar to that of the  $K^+ \rightarrow \pi^+ \pi^- \pi^-$  decay, thus for effective branching ratio we get

$$\text{EBR} = 7 \cdot 10^{-8} \times \text{Efficiency}[\mu^+] \times \text{Efficiency}[\mu^-] \quad (1.24)$$

Rejection of  $\mu^+$  and  $\mu^-$  is expected to be comparable to rejection of  $\pi^+$  and  $\pi^-$  in  $K^+ \rightarrow \pi^+ \pi^+ \pi^-$ , thus we expect the effective branching ratio to be far below  $1 \cdot 10^{-12}$ . In particular, it is expected to be less than than the backgrounds from the  $K^+ \rightarrow \pi^+ \pi^+ \pi^-$  and  $K^+ \rightarrow \pi^+ \pi^- \mu^+ \nu$  decays.

## 1.3.8 Upstream $K^+$ decays backgrounds

In the backgrounds considered so far the  $K^+$  decays have always took place in the fiducial decay volume or, due to finite experimental resolution, just a little bit outside of it. This reflects general feature of a ray trace MC approach: to study effects which, in terms of resolution, are far off the applied cut, it is necessary to devise specific mechanism which would push measured event properties into selected region.

We have identified a possible background scenario, induced by kaon decays upstream of the fiducial decay volume. In this scenario the beam  $K^+$  is still correctly measured by the kaon RICH, so the decay must take place in the last few meters of the kaon RICH or downstream of it. If among the decay products there is a  $\pi^+$ , it can scatter in the BVS. Depending on pion entry point in the BVS and BVS veto thresholds, it can happen that event is not vetoed. When the scattered  $\pi^+$  passes near the beam axis, the reconstruction procedure finds good decay vertex.

This background scenario is illustrated in Fig. 1.15, which shows an event that satisfies all the selection criteria. Other decay products have not been traced. Potentially harmful feature of upstream decays is that the rejection inefficiency of accompanying particles can be many times higher than that for decays in the fiducial volume.

Relevant kaon decays must have large branching ratio and produce a  $\pi^+$ . These are the  $K^+ \rightarrow \pi^+\pi^0$  and  $K^+ \rightarrow \pi^+\pi^+\pi^-$ . We have simulated large number of upstream decays, corresponding to approximately  $36 \cdot 10^6$  decays in the fiducial volume for each of the two decay modes. In the simulation we have enabled multiple scattering everywhere, and hadronic interactions in the BVS only. As a consequence, in this particular simulation actual composition of the BVS matters. We have described it as pure polystyrene, which is not a totally unreasonable approximation. We use GEANT-FLUKA to play hadronic interactions and stop tracking whenever secondary particle is produced. Thus absorption is properly taken into account while simulation is still fast, because events with elastic interactions only survive.

Some distributions for this background are shown in Figs. 1.16 and 1.17. Reconstructed missing mass squared distribution for  $K^+ \rightarrow \pi^+\pi^0$  decays is shown in Fig. 1.16a. All standard event selection cuts, except the cut on missing mass itself, are applied. Figs. 1.16b-d refer to events which fall into either  $K^+ \rightarrow \pi^+\nu\bar{\nu}$  acceptance region. Distribution of the distance the pion passes in the BVS versus  $Z$ -coordinate of the BVS entry point is shown in Fig. 1.16b. True and reconstructed kaon decay vertices are shown in Figs. 1.16c and 1.16d. Analogous distributions for  $K^+ \rightarrow \pi^+\pi^+\pi^-$  decays are shown in Fig. 1.17. The effective background ratio can be expressed in following way:

For the  $K^+ \rightarrow \pi^+\pi^0$  decay

$$\text{EBR(I)} = 6.7 \cdot 10^{-7} \times \text{Efficiency[BVS]} \times \text{Efficiency[Non Veto]} \quad (1.25)$$

$$\text{EBR(II)} = 2.1 \cdot 10^{-6} \times \text{Efficiency[BVS]} \times \text{Efficiency[Non Veto]} \quad (1.26)$$

For the  $K^+ \rightarrow \pi^+\pi^+\pi^-$  decay

$$\text{EBR(I)} = 8.9 \cdot 10^{-8} \times \text{Efficiency[BVS]} \times \text{Efficiency[Non Veto]} \quad (1.27)$$

$$\text{EBR(II)} = 1.5 \cdot 10^{-6} \times \text{Efficiency[BVS]} \times \text{Efficiency[Non Veto]} \quad (1.28)$$

where  $\text{Efficiency[BVS]}$  is probability that an event is not vetoed by the  $\pi^+$  signal in the BVS, and  $\text{Efficiency[Non Veto]}$  is probability that an event is not vetoed by the signal from other decay products. In fact, the two efficiencies are correlated, but our analysis is not yet quite advanced to compute the combined value.

As is seen from Figs. 1.16b and 1.17b, in most background events the pion passes only through part of the BVS. Thus some events may escape rejection even if quite low thresholds are set for the BVS.

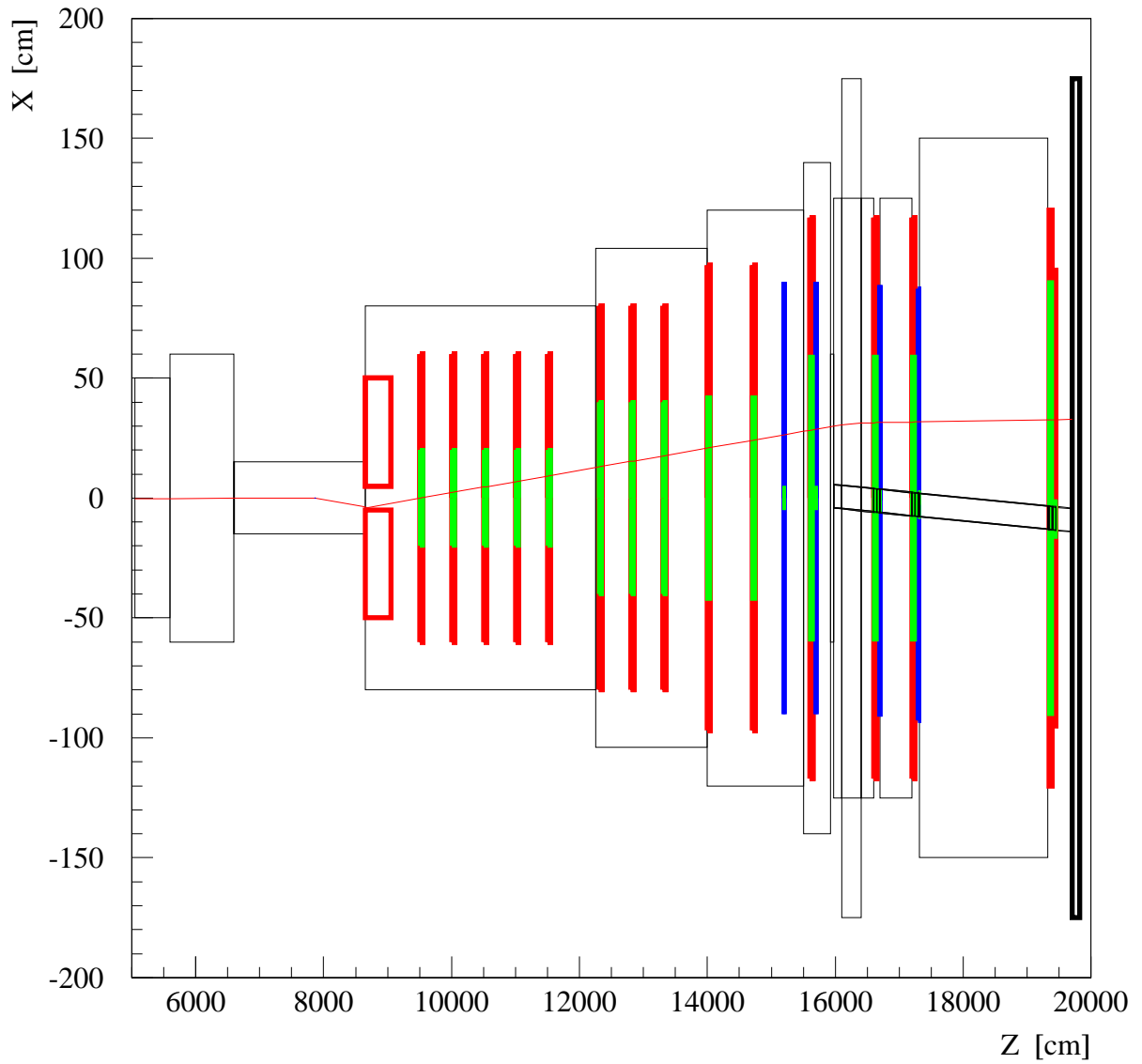


Figure 1.15: Example of a possible upstream  $K^+$  decay background. No other kaon decay products are shown.

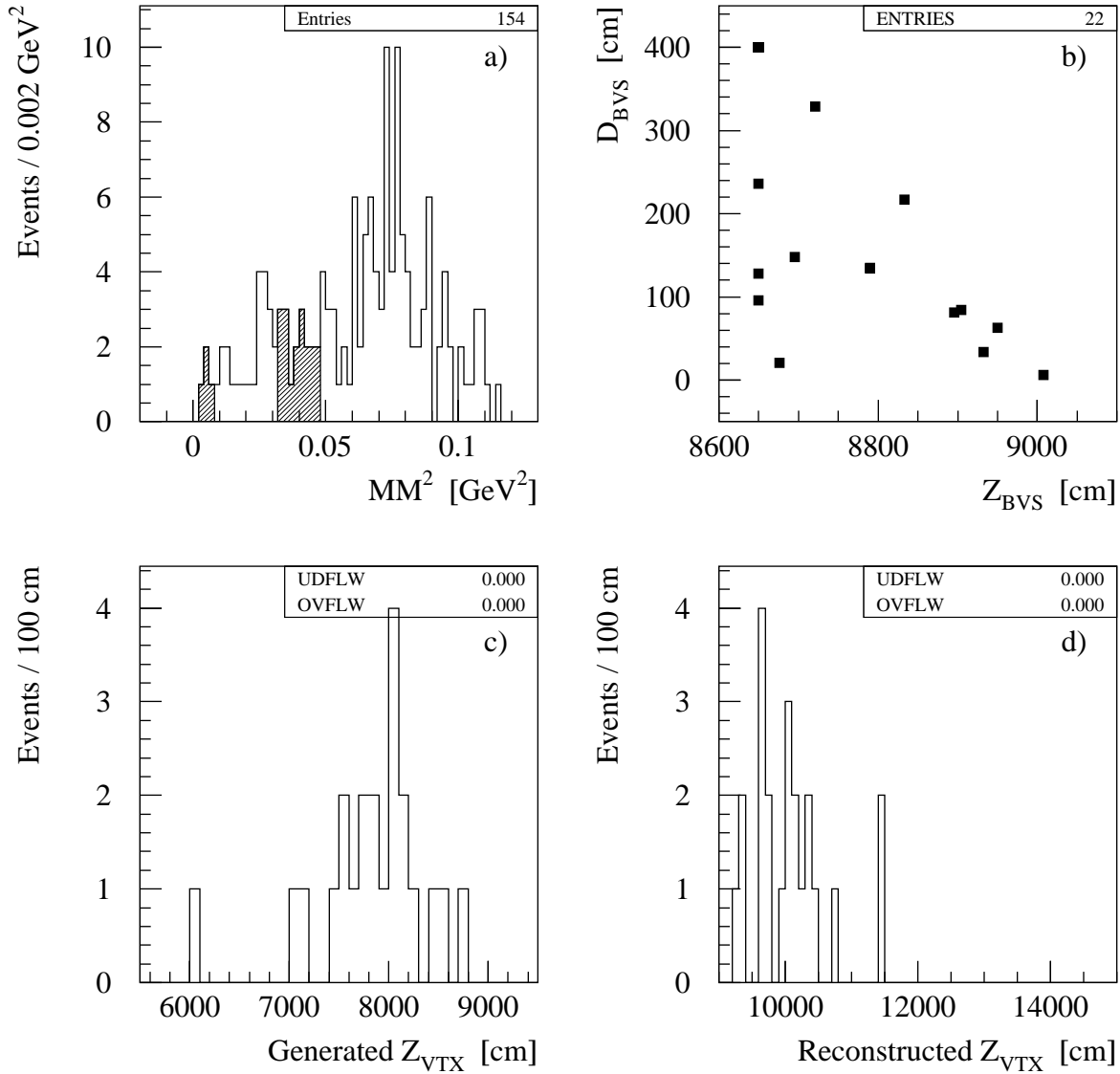


Figure 1.16: Upstream  $K^+ \rightarrow \pi^+ \pi^0$  decays background.

- a) Missing mass squared distribution. Regions I and II are shown hatched.
- b) Distance the pion passes in the BVS versus entry position.
- c)  $Z$ -coordinate of true kaon decay vertex.
- d)  $Z$ -coordinate of the reconstructed decay vertex.

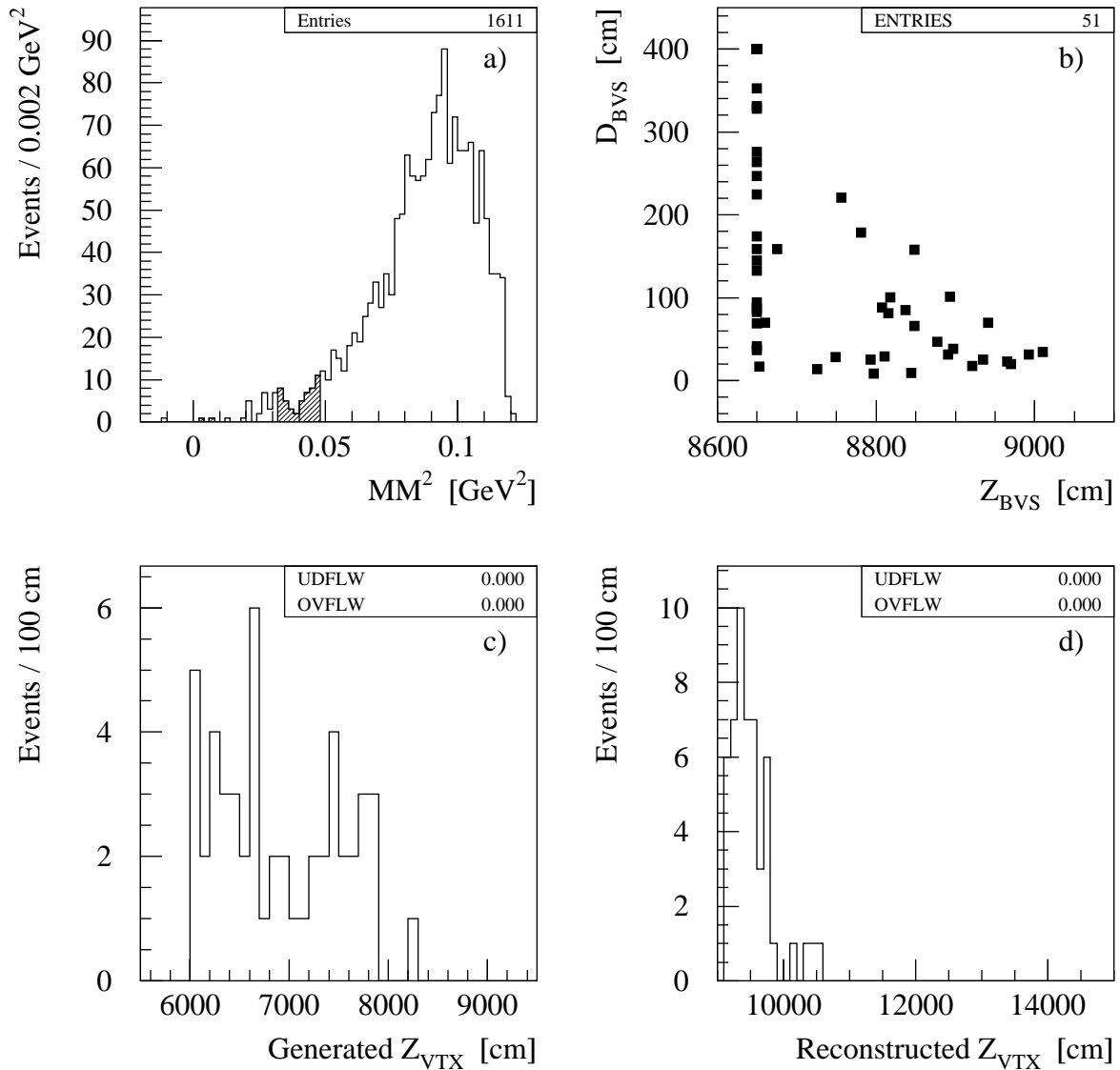


Figure 1.17: Upstream  $K^+ \rightarrow \pi^+ \pi^+ \pi^-$  decays background.  
a) Missing mass squared distribution. Regions I and II are shown hatched.  
b) Distance the pion passes in the BVS versus entry position.  
c)  $Z$ -coordinate of true kaon decay vertex.  
d)  $Z$ -coordinate of the reconstructed decay vertex.

We have not yet made detailed simulations of rejection inefficiency for other decay products. However, decay kinematics allows to make some conclusions. In the  $K^+ \rightarrow \pi^+\pi^+\pi^-$  decay the accompanying  $\pi^+$  and  $\pi^-$  can not escape detector acceptance: they either hit the BVS or enter the decay volume. Thus we expect quite low rejection inefficiency for this upstream decay mode. Situation is different for the  $K^+ \rightarrow \pi^+\pi^0$  decay. Compared to decays in the fiducial volume, the low energy photon has much higher chances to miss a veto. The high energy photon still either hits the BVS, or enters the decay volume. However, it can hit the beam hole or the FVS in the vicinity of the  $\pi^+$  shower, and probabilities of these cases may differ significantly from those of decays in the fiducial volume. This is a question that requires more detailed studies.

## Further comments

At the moment we can not give any trustworthy effective background ratio estimate. In addition to the  $\pi^0$  rejection inefficiency there are many factors which can significantly affect the background estimate: actual beam profile, BVS composition, longitudinal readout segmentation and employed thresholds. Some variations of BVS geometry may also be considered. We believe that with proper optimizations it is possible to keep the upstream decays background at sufficiently low level.

In the most of the background events the pion scatters just on the inner surface of the BVS. Thus, using measured  $\pi^+$  track parameters, we can propagate the track back to the BVS and cut on the transverse position. As such a cut would undoubtedly impact the  $K^+ \rightarrow \pi^+\nu\bar{\nu}$  acceptance, we do not plan to use it unless we are forced to. But this example demonstrates that we do have some tools in reserve.

Another lesson to be learned from the upstream decays is that a  $\pi^+$  scattering in the BVS is a viable mechanism of background creation. Basically any process which can create a pion with momentum of 14–30 GeV is potentially dangerous. And this need not necessarily be a  $K^+$ -induced process, as accidental kaons should often provide a suitable beam track.

## 1.4 Accidental and interaction backgrounds

In this section we consider a few accidental and interaction backgrounds. Because of unseparated beam interaction backgrounds in the P940 are potentially much more dangerous than in the P921. However, in  $\pi^+A$ - and  $pA$ -interactions it is not easy to imitate a  $K^+$  signal in the kaon RICH. It looks more likely that an accidental  $K^+$  can be picked up from the beam. Thus some possible backgrounds are induced both by accidental activity and interactions. That is why it makes some sense to consider these background sources together.

### 1.4.1 Accidentals in the UMS

High beam rate creates wide possibilities for track mismeasurement in the UMS. It can happen that pattern recognition picks up just a few wrong hits, or produces a completely ghost track. To create a background event, however, it is also necessary to have a  $K^+$  in the kaon RICH, and a  $\pi^+$  downstream. Since the kaon RICH responses only to the kaon

component of the beam, it effectively means that there is a real  $K^+$  in the event. Then its decay is the most natural way to create a  $\pi^+$  downstream.

Thus following scenario can lead to background: in an event with a  $K^+$  decay the measurements in the kaon RICH and all downstream of it detectors are basically correct, but the kaon track in the UMS contains wrong hits. Their fraction can vary from 0 to 100%. This is purely accidental background, since it disappears when the rate goes to zero.

Standard  $K^+ \rightarrow \pi^+\nu\bar{\nu}$  event selection procedure requires that time measurements in all four spectrometers are compatible, that momenta in the UMS and kaon RICH agree, and that reconstructed decay vertex is of good quality. After all these selection criteria are applied, the UMS track parameters in the selected events are quite close to that of original  $K^+$  track. This is true even for tracks, composed completely of wrong hits. Stand-alone simulations [10] show that though the reconstructed missing mass squared is mismeasured a little, it is quite close to the true value. Thus the background scenario being considered contributes only to those kaon decay backgrounds, rejection of which strongly relies on good missing mass squared resolution. In practice that means only the  $K^+ \rightarrow \pi^+\pi^0$  background, and mainly for region I.

We have performed stand-alone simulations, in which we have applied full UMS track reconstruction to  $K^+ \rightarrow \pi^+\pi^0$  decays. We have found that at the nominal beam rate of 250 MHz the probability that reconstructed missing mass squared falls into selected region is  $1.3 \cdot 10^{-5}$  for region I and  $3.1 \cdot 10^{-6}$  for region II. These rejection inefficiencies are small compared to those in the "classical"  $K^+ \rightarrow \pi^+\pi^0$  background. Using obtained numbers in expressions (1.14) and (1.15) for the  $K^+ \rightarrow \pi^+\pi^0$  background (page 16), we get:

$$\text{EBR(I)} = \frac{0.2116 \times 0.263 \times 1.3 \cdot 10^{-5} \times 1.0 \cdot 10^{-7}}{0.035} = 2.0 \times 10^{-12} \quad (1.29)$$

$$\text{EBR(II)} = \frac{0.2116 \times 0.218 \times 3.1 \cdot 10^{-6} \times 1.0 \cdot 10^{-7}}{0.050} = 0.3 \times 10^{-12} \quad (1.30)$$

## 1.4.2 Accidentals in the UMS and kaon RICH

In the previous subsection we have considered accidental background, induced by wrong  $K^+$  measurement in the UMS, but correct  $K^+$  measurement in the kaon RICH. Now we consider a case when  $K^+$  measurement in the kaon RICH is also wrong. A simple and plausible way to make such a mistake is to measure another (accidental)  $K^+$ . Thus, we assume that there are two close in time beam  $K^+$  particles. One of them is correctly measured by the UMS and kaon RICH. The other, which is not seen by the RICH, produces  $\pi^+$  in the decay volume. How can it be that a  $K^+$  is not seen by the kaon RICH? Statistical fluctuations in the number of photoelectrons is a conceivable reason.

Standard event selection procedure requires that there is no accidental activity in veto detectors. In the first approximation that means that the  $K^+$  which has been measured by the kaon RICH must not decay in the setup, otherwise an event is more likely to be rejected. We do not use this rejection, which is about 0.7–0.9, and which is different for regions I and II, in further calculations. We do not expect any changes in rejection of decay products which accompany the  $\pi^+$ . Rejections based on event kinematics must be simulated. In simulations we need to consider only those  $K^+$  decays, in which the missing mass squared selection plays an important role. These are the  $K^+ \rightarrow \pi^+\pi^0$  and  $K^+ \rightarrow \pi^+\pi^+\pi^-$  decays.

We have studied both decays. In simulations we have forced the first  $K^+$  not to decay, while the second  $K^+$  has been forced to decay in the region  $6000 < Z < 15500$  cm. This decay region extends far upstream and a little downstream of the fiducial one. This is done to allow for vertex position misreconstructions, which are likely in this kinematics. But the acceptance is still defined with respect to kaon decays in the fiducial volume. For the  $K^+ \rightarrow \pi^+\pi^0$  decay we have obtained an acceptance of 0.52% for region I and 0.30% for region II. For the  $K^+ \rightarrow \pi^+\pi^+\pi^-$  decay we have obtained much smaller values of  $< 2 \cdot 10^{-5}$  for region I and  $4 \cdot 10^{-5}$  for region II.

Missing mass squared distribution for events which pass all standard selection criteria, except the cut on missing mass squared itself, is shown in Fig. 1.18a for region I and in Fig. 1.18b for region II. These distributions quite well follow normal distribution with mean  $\mu = m_{\pi^0}^2$  and root mean square deviation  $\sigma = 9 \cdot 10^{-3} \text{ GeV}^2$ . Distribution of the true  $Z$ -coordinate of the decay vertex for background events is shown in Fig. 1.18c. One can see that in almost all background events the  $K^+ \rightarrow \pi^+\pi^0$  decay takes place in the fiducial decay volume, and in very few events just upstream of it. There are no events with far upstream decays. Therefore we may apply the same  $\pi^0$  rejection inefficiency as has been determined for the  $K^+ \rightarrow \pi^+\pi^0$  background. We have also studied the decay vertex  $Z$ -position resolution. We have found that difference between the reconstructed  $Z$ -coordinate of the decay vertex and its true value is reasonably well described by the normal distribution with mean  $\mu = -70$  cm and root mean square deviation  $\sigma = 320$  cm.

Acceptance for the background from the  $K^+ \rightarrow \pi^+\pi^+\pi^-$  decays is negligible compared to that from the  $K^+ \rightarrow \pi^+\pi^0$  decays. The largest rejection comes from the missing mass squared cut, as demonstrated in Fig. 1.18d. It has turned out that the  $9 \cdot 10^{-3} \text{ GeV}^2$  resolution is sufficiently good to protect region II. Combining obtained  $K^+ \rightarrow \pi^+\pi^0$  acceptances with branching ratio of the decay,  $\pi^0$  rejection inefficiency and  $K^+ \rightarrow \pi^+\nu\bar{\nu}$  acceptances, we can express effective branching ratios as

$$\text{EBR(I)} = 3.1 \cdot 10^{-9} \times \text{Efficiency[Time]} \times \text{Efficiency[RICH]} \quad (1.31)$$

$$\text{EBR(II)} = 1.3 \cdot 10^{-9} \times \text{Efficiency[Time]} \times \text{Efficiency[RICH]} \quad (1.32)$$

Multiplying the nominal kaon rate of 10 MHz by the 6 ns ( $\pm 3$  ns) time window, we get  $\text{Efficiency[Time]} = 0.06$ . Thus to keep the effective background ratio below the  $10^{-12}$  level, we need to keep the  $\text{Efficiency[RICH]}$ , which is the probability that kaon signal in the RICH does not veto an event, below 0.5%. To calculate expected probabilities, we approximate dependence of the average number of photoelectrons in the kaon RICH on momentum with a linear function, equal to 7 and 14 at 37 and 53 GeV correspondingly. This is slightly worse than expected performance [2]. We get the probability of 0.01% for response of 0 photoelectrons, 0.12% for no more than 1, 0.54% for no more than 2, 1.7% for no more than 3, 4.1% for no more than 4. In a conservative approach of accepting events with 2 accidental hits in the kaon RICH we get

$$\text{EBR(I)} = 1.0 \times 10^{-12} \quad (1.33)$$

$$\text{EBR(II)} = 0.4 \times 10^{-12} \quad (1.34)$$

It is not clear whether global inefficiency considerations will allow to use more stringent cut of no more than 1 accidental hit. However, it seems likely that timing cut can be made tighter, reducing the background a little.

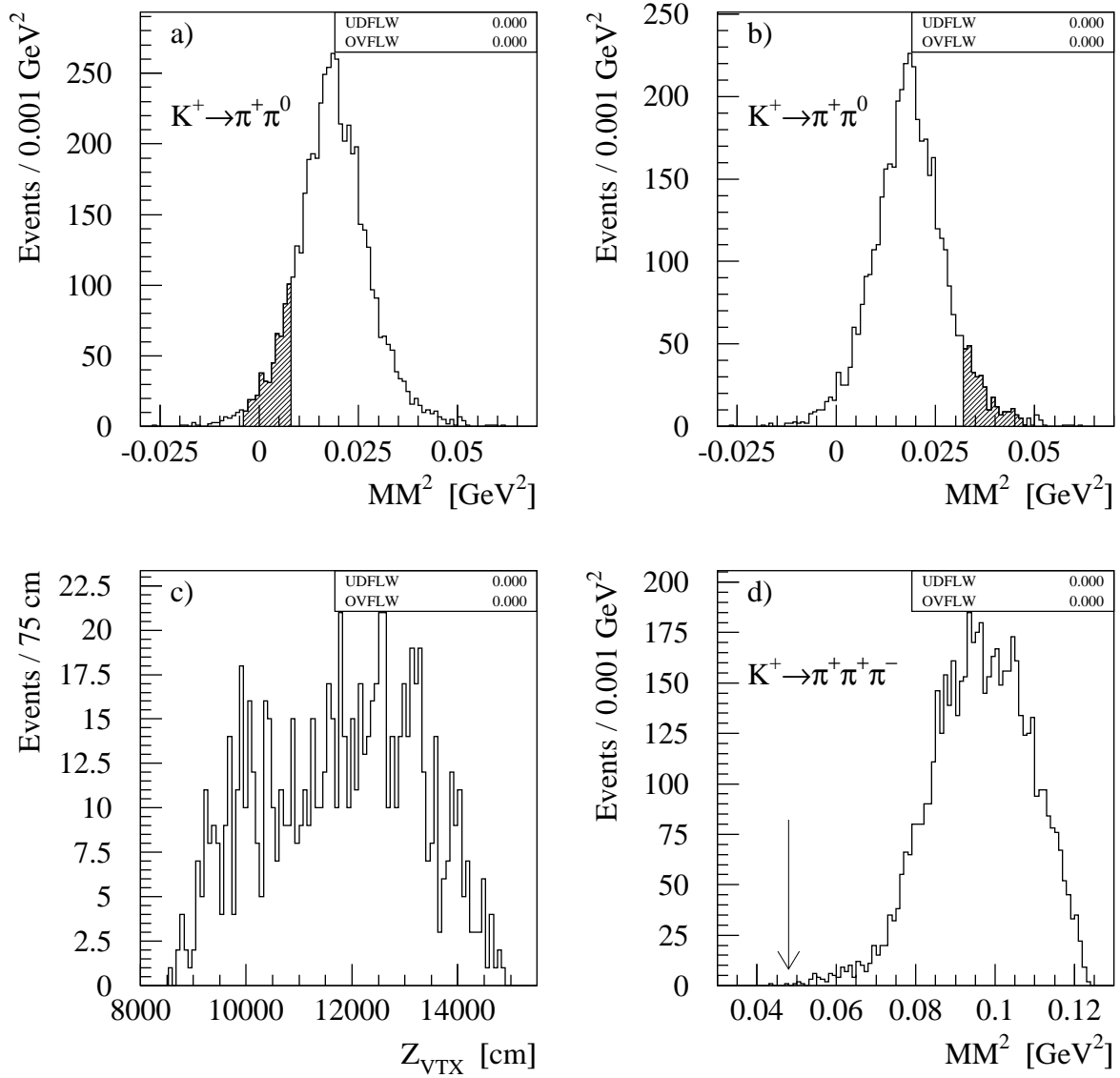


Figure 1.18: Accidentals in the UMS and kaon RICH.  
a), b) Missing mass squared distributions in region I and II for accidentals with the  $K^+ \rightarrow \pi^+\pi^0$  decays. All cuts are applied, except for the  $MM^2$ .  
c) True  $Z$ -coordinate of the decay vertex for background events.  
d) Missing mass squared distribution for accidentals with the  $K^+ \rightarrow \pi^+\pi^+\pi^-$  decays. The arrow shows region II upper limit.

### 1.4.3 The $K^+$ residual gas interactions

This background is a result of  $K^+$  interactions with residual gas in the vacuum decay volume which produce a  $\pi^+$  that falls into detector acceptance. The only way to reject that background is to veto on other interaction products. But it is also possible to avoid the background by keeping a good vacuum.

#### Cross section

In the previous editions of the proposal the  $K^+$  interaction length in air at 1 atm has been assumed to be 470 m. In the process of verification of basic assumptions we have found that this value is not correct.

The most precise data on  $K^+$ -nucleus inelastic interactions [11] have better than 10% accuracy. The measurements refer to the energies of 30 and 50 GeV. It has been found that, within experimental errors, the cross section is constant at these energies. We have interpolated data for different nuclei to the average atomic number of air  $A = 14.61$  and obtained

$$\sigma_{\text{inel}}[K^+ \text{ Air}] \approx 180 \text{ mbarn} \quad (1.35)$$

This corresponds to mean path between inelastic collisions

$$\lambda = \frac{1}{\sigma(\rho N_A/A)} = 1120 \text{ m} \quad (1.36)$$

Scaling the PDG value of nuclear interaction length for air  $\lambda_I = 90.0 \text{ g/cm}^2$ , which corresponds to protons and neutrons, by a factor of 3/2 to account for smaller kaon cross section, we get an interaction length of about 1100 m. Finally, we have looked at values given by GEANT. For kaon energies of approximately 45 GeV GEANT-FLUKA gives mean path between interactions of 1150 m, while GEANT-GHEISHA gives 1160 m. Therefore we conclude that  $\lambda = 1120 \text{ m}$  is the right estimate.

#### Expected background level

Combining the estimated  $K^+$  interaction length in air at 1 atm (760 torr), residual pressure of  $1 \cdot 10^{-6}$  torr, decay base of 59 m for region I and 44 m for region II, decay fraction of 0.16, and acceptance values of 3.5% and 5.0% for regions I and II, we can express effective background ratios as follows:

$$\text{EBR(I)} = 1.2 \cdot 10^{-8} \times \text{Efficiency}[\pi^+] \times \text{Efficiency}[\text{Non Veto}] \quad (1.37)$$

$$\text{EBR(II)} = 6.5 \cdot 10^{-9} \times \text{Efficiency}[\pi^+] \times \text{Efficiency}[\text{Non Veto}] \quad (1.38)$$

where  $\text{Efficiency}[\pi^+]$  is probability that interaction results in a  $\pi^+$  which would satisfy all the selection criteria, and  $\text{Efficiency}[\text{Non Veto}]$  is probability that all other interaction products do not veto the event.

To estimate fraction of inelastic interactions which produce suitable  $\pi^+$  we extrapolate the Single Arm Spectrometer measurements of inclusive  $\pi^+$  production [12, 13]. We define  $\pi^+$  as suitable if its momentum is between 14 and 30 GeV and if missing mass squared is in

region I or II. We have obtained a fraction of 0.2% for region I and 0.3% for region II. Pions which satisfy two stated conditions are very likely to pass all other selection cuts as well, and we expect any further rejections to be less than a factor of 2.

It may be interesting to make a comparison with the P921 option. Using the same extrapolation, we have obtained a value of 0.03% for region I. The difference is likely to be caused by the fact that P940 and P921 options use different pion  $x_F$  regions. Incidentally, the latter number is in a reasonable agreement with FRITIOF simulations, which have been done for the first edition of the CKM proposal. In those calculations a value of 0.015% has been obtained for events with all kinematic selections applied.

Given that  $\text{Efficiency}[\pi^+] \approx 0.2\%$ , rejection inefficiency of other interaction products less than 0.04 is required to keep the overall effective branching ratio below  $10^{-12}$  level. Event selection cuts on  $K^+$  and  $\pi^+$  momenta guarantee that the total energy of accompanying particles is in the 7–39 GeV range. Evidently typical interactions are vetoed orders of magnitude better than required. However, there may exist processes which are more difficult to reject. Production of  $K_L^0\pi^+$ , where  $K_L^0$  passes through the FVS and is absorbed in the MVS, is an example. Effective background ratios of such processes depend on their cross sections and details of production kinematics. These can not be reliably determined in simulations and ultimately must be measured. Still, intuition suggests that  $\text{EBR} < 1 \cdot 10^{-12}$ .

## 1.5 Rates in detectors and associated inefficiency

In this section we assume following beam composition: 10 MHz  $K^+$ , 100 MHz  $\pi^+$ , 132 MHz  $p$ . An issue of rates in a 250 MHz beam certainly deserves careful consideration. First, there is a concern about detector performance in a high rate environment. Second, there is a concern about inefficiency caused by accidental hits.

However, only the UMS chambers see the full beam intensity. The kaon RICH sees only the  $K^+$  component, since protons are under the Cherenkov radiation threshold, while area, which the pion Cherenkov radiation is focused to, is not instrumented. No other detector is instrumented in the beam line, including the pion RICH, which is crossed by a vacuumed beam pipe. The BVS, VVS, SVS, FVS, MVS, DMS and pion RICH are affected by  $\pi^+$ -decays,  $K^+$ -decays, and beam interactions.

### 1.5.1 Global inefficiency

Rates for veto detectors are threshold dependent. The VVS modules will use thresholds, corresponding to 60–120 MeV photons. This is likely to be below one MIP. Thus in a first approximation a charged particle, hitting a VVS module, vetoes each event. For the purpose of this estimate we assume the same to be true for the BVS. As for other detectors, the selection criteria depend on whether the  $K^+ \rightarrow \pi^+\nu\bar{\nu}$  candidate belongs to the region I or II. We plan to set thresholds in the SVS and FVS sufficiently high, so that one MIP signals do not veto region I events but veto (most of) region II ones. Also, region I events are quite insensitive to accidental hits in the DMS straw tubes and in the pion RICH, while region II events are rejected because of the  $K^+ \rightarrow \pi^+\pi^-e^+\nu$  background.

To estimate rates due to decays we have simulated beam particles as originating from  $Z =$

3600 cm, which is approximately the position of the last beam collimator. Four magnets, placed over approximately 15m downstream of that collimator, absorb low energy decay products, but are not implemented in the simulation program. However, 15m is a small number compared to the full setup length. We have considered only the  $\pi^+ \rightarrow \mu^+\nu$  and  $K^+ \rightarrow \mu^+\nu$  decays. In case of kaons it is certainly not the best of approximations, since there are decays which produce photons or more than one charged particle. These do increase rate per detector channel, however, do not significantly change event veto rate: all decay products are synchronous in time, and once an event is rejected, it does not matter how many times. Besides, fraction of all other kaon decays is only 36%. Also, to take into account higher FVS threshold for region I events, we veto an event with 36% probability if a muon from the  $K^+ \rightarrow \mu^+\nu$  decay hits the FVS. We think that our estimates are accurate to about 25%.

To estimate rates due to interactions of beam particles we assumed that basically each interaction which occurs in the last UMS chamber or downstream of it produces a signal in the BVS and thus vetoes an event. We estimate that that region contains 0.55% of interaction length. We also use a factor of 2/3 for meson cross sections.

Event veto rates for each  $K^+ \rightarrow \pi^+\nu\bar{\nu}$  region and for each of the discussed mechanisms are summarized in Table 1.5.

Process	Region I	Region II
$\pi^+$ decays	0.12	4.08
$K^+$ decays	2.24	3.41
Interactions	1.16	1.16

Table 1.5: Event veto rates [MHz].

To determine actual inefficiencies, we use a time window of 6 ns ( $\pm 3$  ns) for vetoes, induced by decays. Interactions, however, can produce sufficiently energetic particles to fire a veto but slowly moving to arrive out of time. To account for this we use twice as large time window of 12 ns for interactions. These assumptions give 3% global inefficiency for region I and 6% for region II.

## Caveats

The time window of 12 ns for vetoes induced by interactions has been chosen quite arbitrarily. Actual effective time window clearly depends on the threshold, which should not necessarily be the same for all parts of the BVS. The issue of thresholds and rates in the BVS deserves further studies, preferably in test beam.

### 1.5.2 Rates in the DMS and FVS

In the first approximation we can neglect contribution of beam interactions, since solid angle, covered by the DMS stations and viewed from possible vertex positions, is rather small. The second approximation we make is that for kaons we generate only the  $K^+ \rightarrow \mu^+\nu$  decays, but with 100% branching ratio. Rate per tube for non-bending plane is shown in Fig. 1.19.

The rate is maximal for tubes which are concentrated around the beam. It is determined by pion decays and equals about 100 kHz. Clearly, the result depends on the actual beam profile and halo. Nonetheless it is likely the tubes can be moved closer to the beam axis, improving the  $K^+ \rightarrow \pi^+ \nu \bar{\nu}$  and  $K^+ \rightarrow \pi^+ \pi^- e^+ \nu$  separation in the region II.

Rate in the central part of the FVS is shown in Fig. 1.20. The calculation is done for  $5 \times 5 \text{ cm}^2$  counters. The rate is maximal near the beam hole, where it is about 250 kHz. Real rate is expected to be higher, since muon bremsstrahlungs and hadron interactions in the material of the beam pipe produce multichannel showers instead of MIP signals. However, counters of  $2.5 \times 2.5 \text{ cm}^2$  reduce the rate.

We plan to use the former KTeV CsI calorimeter as the FVS. This is quite slow device. The question is how good can it reject MIP signals (as is necessary to suppress the  $K^+ \rightarrow \pi^+ \pi^- e^+ \nu$  background) around the beam hole.

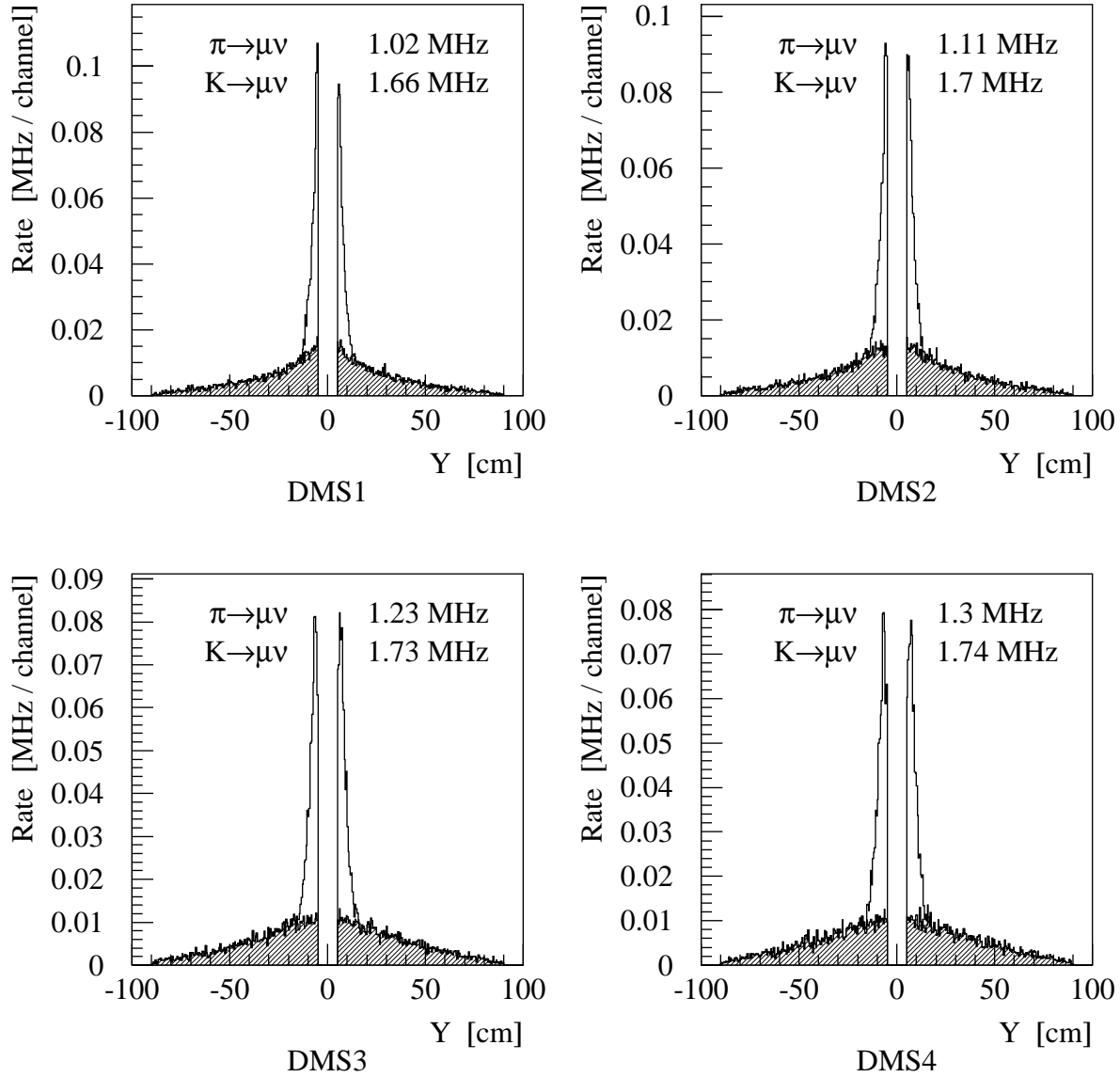


Figure 1.19: Rate per tube in the DMS for non-bending plane. Kaon decays are 100%  $K^+ \rightarrow \mu^+\nu$ . Kaon contribution is hatched. Numbers show total rate for a decay.

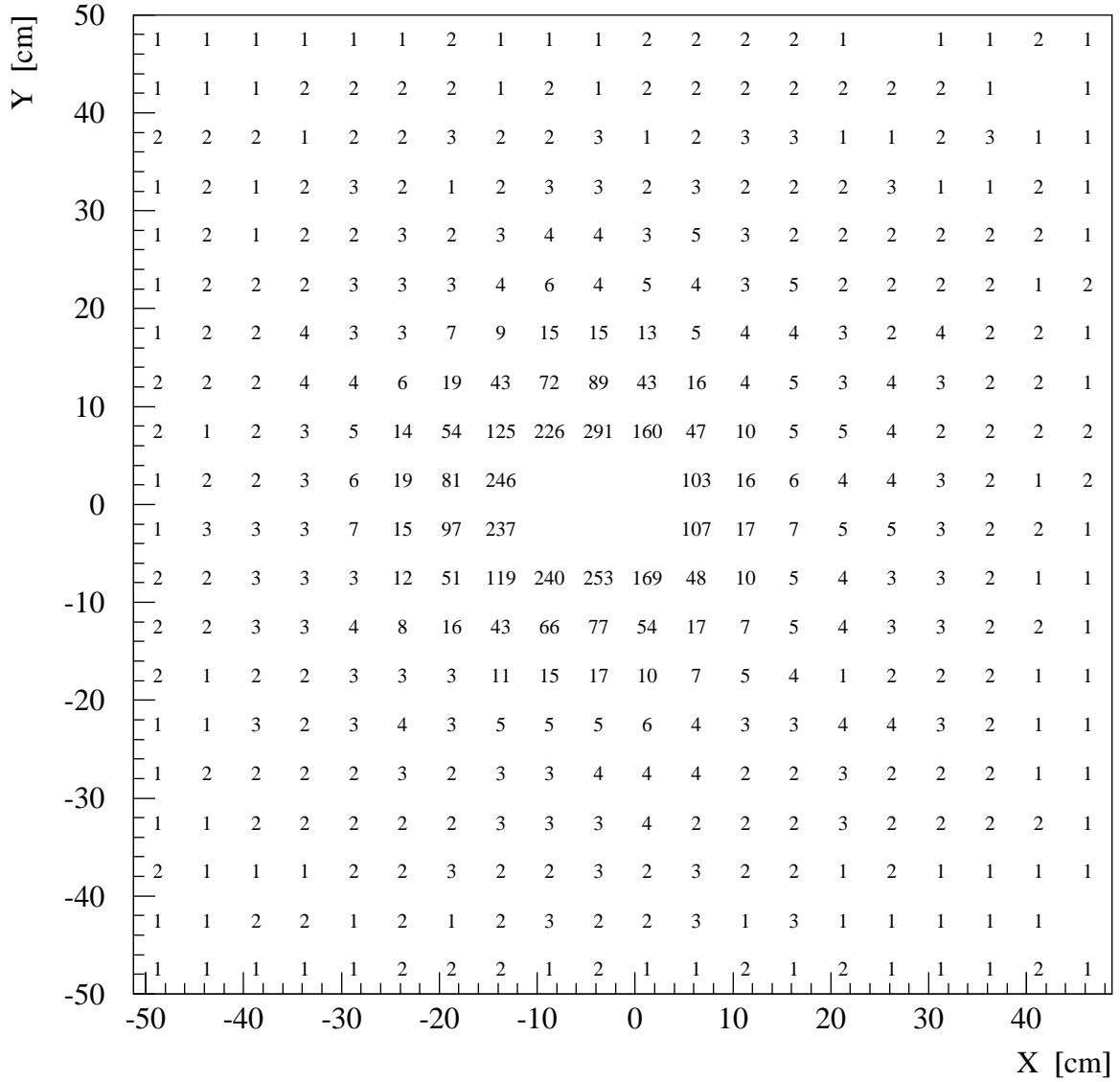


Figure 1.20: Rate in the FVS central part [kHz]. Counters  $5 \times 5 \text{ cm}^2$  are assumed. Kaon decays are 100%  $K^+ \rightarrow \mu^+ \nu$ .

## 1.6 Summary

We summarize our background studies in Table 1.6. We have considered all kaon decays, and have come to conclusion that the  $K^+ \rightarrow \pi^+\pi^0$  decay is the main source of background for region I, while the  $K^+ \rightarrow \pi^+\pi^-e^+\nu$  decay is the most problematic one for region II. We have considered few accidental and interaction backgrounds and identified no significant problems so far.

Background Process	EBR (in units of $10^{-12}$ )	
	Region I	Region II
$K^+ \rightarrow \mu^+\nu$	$< 1$	—
$K^+ \rightarrow \pi^+\pi^0$	9.5	1.1
$K^+ \rightarrow \pi^+\pi^0\gamma$	—	4.4
$K^+ \rightarrow \pi^+\pi^-e^+\nu$	—	25
Other $K^+$ decays	$\ll 1$	$< 1$
Accidentals in the UMS	2.0	0.3
Accidentals in the UMS and kaon RICH	1.0	0.4
Total	13	31

Table 1.6: Summary of backgrounds.

The study of backgrounds is not complete. We can not claim that we have addressed all the backgrounds, caused by pattern recognition errors and non-gaussian resolution effects. Accidental and interaction backgrounds have been considered rather briefly. However, these can not be determined with confidence in simulations only, and better be measured. In a sense, study of backgrounds can not be completed until the experiment is done!

We are now quite confident in our ability to handle region II. We do not expect any new backgrounds, associated with kaon decays. It does not mean that some intricate interaction background can not exist which we have failed to anticipate. But if it does, a-priory it is equally likely to affect region I as well as region II.

In the used framework of ray trace MC we have simulated only a few aspects of event generation and reconstruction, which are directly relevant to background studies. That is why a probability to detect a  $K^+ \rightarrow \pi^+\nu\bar{\nu}$  event once it has occurred, or efficiency, is less than an obtained in simulations value, which we refer to as acceptance. Factors, causing additional inefficiency, and their expected impact, are collected in Table 1.7. They have been determined in stand-alone simulations, analyses of experimental data, or just invented with educated guess. In general, selections designed to veto background contributions use different cut values in regions I and II, and corresponding efficiencies are different as well.

Now we are in position to estimate the absolute  $K^+ \rightarrow \pi^+\nu\bar{\nu}$  yield. We use following parameters and assumptions:

- 39 weeks of running per year
- 120 hours of running per week
- 3600 seconds per hour
- 6 seconds flat top out of 28 seconds spill
- 10 MHz  $K^+$  rate

Origin of Inefficiency	Efficiency	
	Region I	Region II
Track reconstruction in UMS	90%	90%
Track reconstruction in kaon RICH	92%	92%
Momentum agreement for kaon track in UMS and RICH	99%	99%
Pattern recognition in DMS	98%	98%
Track reconstruction in pion RICH	98%	98%
Time agreement between UMS, DMS, pion and kaon RICHes	96%	96%
Pion identification in MVS	90%	99%
Pion signal in FVS is not like $\gamma$	98%	—
Pion signal in FVS is not like $\pi^+\gamma$	90%	90%
Pion signal in FVS is not like $\pi^+\pi^-$	—	95%
No accidentals in BVS, VVS, SVS, FVS, DMS, pion RICH	97%	94%
<b>Total</b>	<b>58%</b>	<b>60%</b>

Table 1.7: Factors and efficiencies not simulated.

- Decay fraction of 0.16
- Acceptances of 3.5% and 5% for regions I and II
- Additional efficiency factors of 58% and 60% for regions I and II
- Branching ratio of  $1 \cdot 10^{-10}$

Multiplying all the values, we obtain 12 signal events per year for region I and 17 signal events per year for region II. Assuming 3 years of running we get 87 signal events and 21 background ones. All the numbers are pulled together in Table 1.8. Cut optimization for the region II is likely to raise the signal a little and/or lower the background.

<b>YIELDS</b>	1 Year		3 Years	
	Signal	Background	Signal	Background
Region I	11.7	1.5	35.2	4.6
Region II	17.3	5.4	52.0	16.1
<b>Total</b>	<b>29</b>	<b>6.9</b>	<b>87</b>	<b>21</b>

Table 1.8: Event yields per one and three years of data taking.

# Bibliography

- [1] H. Nguyen, private communication.
- [2] P. Cooper, Redesign of the CKM RICH Velocity Spectrometers for use in a  $1/4$  GHz beam, talk at RICH2004.
- [3] J. Frank et al., Charged Kaons at the Main Injector, A Proposal for a Precision Measurement of the Decay  $K^+ \rightarrow \pi^+ \nu \bar{\nu}$  and Other Rare Processes at Fermilab Using the Main Injector, 2nd Edition, Fermi National Accelerator Laboratory, Batavia, IL, USA, April, 2001.
- [4] A. Morelos et al., Radial Tail Resolution in the SELEX RICH, to be published in RICH2004 proceedings.
- [5] L. Maiani (ed.), G. Pancheri (ed.) and N. Paver (ed.). The second DAPHNE physics handbook. Vol. 1, 2. Frascati, Italy: INFN (1995) 1202 p.
- [6] S. C. Adler *et al.*, “Measurement of direct photon emission in  $k^+ \rightarrow \pi^+ \pi^0 \gamma$  decay,” *Phys. Rev. Lett.*, vol. 85, pp. 4856–4859, 2000.
- [7] P. Kitching *et al.*, “Observation of the decay  $k^+ \rightarrow \pi^+ \gamma \gamma$ ,” *Phys. Rev. Lett.*, vol. 79, pp. 4079–4082, 1997.
- [8] R. Appel *et al.*, “A new measurement of the properties of the rare decay  $k^+ \rightarrow \pi^+ e^+ e^-$ ,” *Phys. Rev. Lett.*, vol. 83, pp. 4482–4485, 1999.
- [9] H. Ma *et al.*, “A new measurement of the rare decay  $k^+ \rightarrow \pi^+ \mu^+ \mu^-$ ,” *Phys. Rev. Lett.*, vol. 84, pp. 2580–2583, 2000.
- [10] H. Nguyen, CKM note 101.
- [11] Y. P. Gorin *et al.*, “Nuclear absorption cross-sections for pions, kaons, protons, and anti-protons in the momentum range 6-60  $\text{gev}/c$ ,” *Yad. Fiz.*, vol. 18, pp. 336–347, 1973.
- [12] A. E. Brenner *et al.*, “Experimental study of single particle inclusive hadron scattering and associated multiplicities,” *Phys. Rev.*, vol. D26, p. 1497, 1982.
- [13] D. S. Barton *et al.*, “Experimental study of the a-dependence of inclusive hadron fragmentation,” *Phys. Rev.*, vol. D27, p. 2580, 1983.